GEOLOGICA BELGICA (2010) 13/1-2: 91-112

GEOLOGY OF THE CASSITERITE MINERALISATION IN THE RUTONGO AREA, RWANDA (CENTRAL AFRICA): CURRENT STATE OF KNOWLEDGE

Stijn DEWAELE[1], Friso DE CLERCQ[2], Philippe MUCHEZ[2], Jens SCHNEIDER[2], Ray BURGESS[3], Adrian BOYCE[4] & Max FERNANDEZ ALONSO [1]

(8 Figures, 5 Tables and 2 Plates)

1. Department of Geology and Mineralogy, Royal Museum for Central Africa, Leuvensesteenweg 13, B-3080 Tervuren, Belgium. E-mail: Stijn.Dewaele@africamuseum.be
2. Geodynamics & Geofluids Research Group, Katholieke Universiteit Leuven, Celestijnenlaan 200E, B-3001 Leuven, Belgium
3. University of Manchester, School of Earth, Atmospheric and Environmental Sciences, Oxford Road, Manchester M13 9PL, United Kingdom
4. Scottish Universities Environmental Research Centre, Rankine Avenue, Scottish Enterprise Technology Park, East Kilbride G75 0QF, Scotland, UK

ABSTRACT. The Mesoproterozoic Kibara orogen in Central Africa hosts different granite-related rare element deposits that contain cassiterite, columbite-tantalite ("coltan"), wolframite, beryl, spodumene, etc. as typical minerals. The primary deposits of these minerals are formed by pegmatites and quartz veins that have historically been related to the youngest, most evolved G4-granite generation in the northern part of the Kibara orogen. This study focuses on quartz vein-type cassiterite mineralisation in the Rutongo area in Rwanda.
The Rutongo area consists of a large anticline that is characterised by the presence of cassiterite-mineralised quartz vein sets that dominantly occur in quartzites. The emplacement of the quartz veins has been related to a later phase in the deformation history of the Kibara orogeny. The mineralised quartz veins are associated with intense alteration, comprising silicification, tourmalinisation, sericitisation and muscovitisation. Cassiterite itself is associated with muscovite in fractures in and along the margins of the quartz veins. Cassiterite crystallisation is followed by the precipitation of different sulphides, such as arsenopyrite, pyrite, chalcopyrite and galena. Cassiterite mineralisation resulted from the circulation of high-temperature and moderate-salinity fluids with a H_2O-CO_2-(CH_4-N_2)-NaCl composition. The stable isotopic composition of the cassiterite mineralising fluids indicates precipitation during metamorphic hydrothermal conditions, during which the metamorphic fluids where in isotopic equilibrium with granitic rocks. The circulation of these fluids probably resulted in the remobilisation of the Sn from these magmatic rocks, as indicated by the relative low Sn concentration of the specialised G4-granites. ^{40}Ar-^{39}Ar age dating of muscovite associated with the mineralisation gives an integrated age of 869 ± 7 Ma, which is clearly younger than the age of the G4-granites (~986 Ma) and the pegmatites with associated columbite-tantalite mineralisation (~965 Ma) in the area. Based on this large time gap, the ^{40}Ar-^{39}Ar age is interpreted to reflect a hydrothermal event post-dating the emplacement of the Kigali granite, only indicating a possible minimum age for the formation of the cassiterite mineralisation.
Based on the structural setting, petrographical observations, the geochemistry of the G4-granites, stable isotope geochemistry, we therefore propose a model in which Sn was mobilised from primary magmatic rocks by a metamorphic hydrothermal fluid system that was generated after crystallisation of the granites and pegmatites. Cassiterite was precipitated in structurally controlled locations, together with the alteration of the host-rocks.

KEYWORDS: Kibara orogen, Rutongo area, cassiterite, stable and lead isotopes, ^{40}Ar-^{39}Ar age dating

1. Introduction

The Central African Mesoproterozoic Kibara orogen extends from Katanga (Democratic Republic of Congo, DRC) in the south to southern Uganda in the north. This orogenic belt forms a large metallogenic province that contains numerous granite-related ore deposits, which are rich in minerals like cassiterite (SnO_2), columbite-tantalite (also called coltan, $(Nb,Ta)_2O_5$), wolframite ($(Fe,Mn)WO_4$), beryl ($Be_3Al_2Si_6O_{18}$), spodumene ($LiAlSi_2O_6$), amblygonite ($(Li,Na)AlFPO_4$), monazite ($(Ce,La,Y,Nd,Th)PO_4$), gold (Au), etc. The presence of these mineral deposits plays an important role in the numerous conflicts in this Central African area, which generate important socio-economic and humanitarian problems. The minerals are present in different types of mineralisation. They occur as primary mineralisation in quartz veins, greisens and pegmatites, but also as secondary mineralisation in alluvial or eluvial deposits.

This article is focussing on the cassiterite mineralisation present in the Rutongo area (Fig. 1), which can be

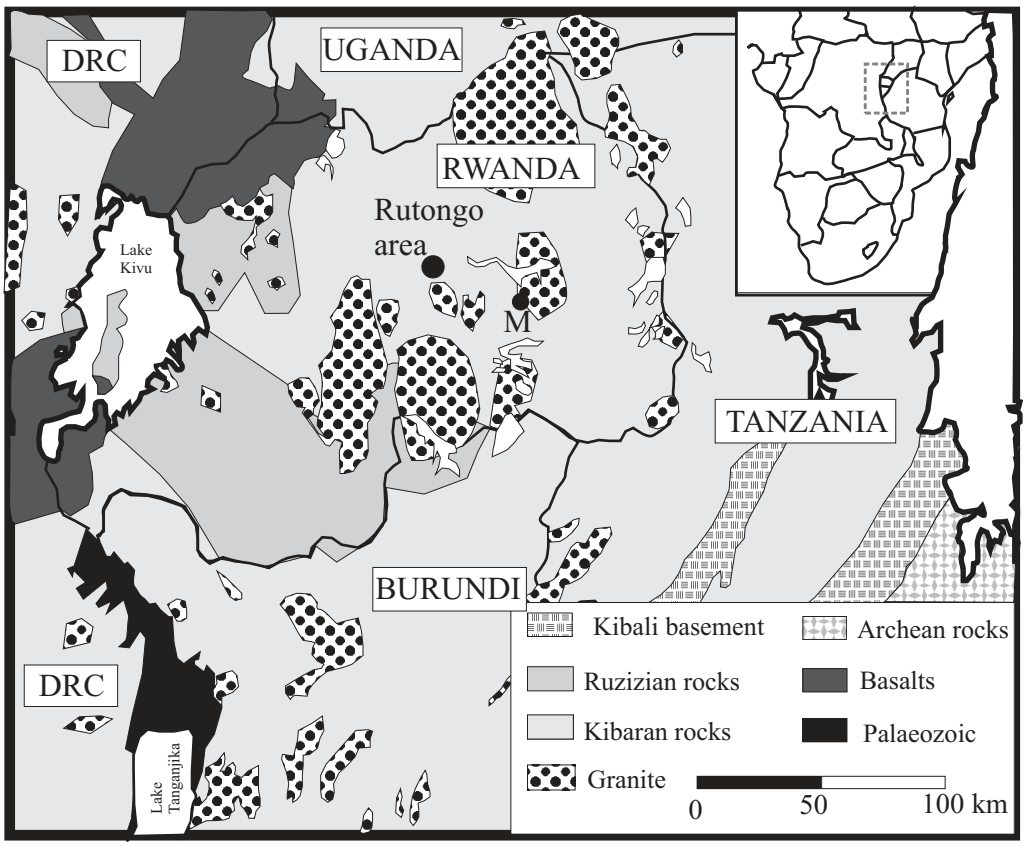

Figure 1. Simplified geological map of Rwanda (after maps KMMA-Rwanda). Location of the Rutongo area and of Musha (M) is indicated by dots.

considered as representative for primary vein-type cassiterite mineralisation in the Kibara orogen. The Rutongo area is situated in the central part of Rwanda, about 10 km north of Kigali. Exploration and exploitation started in the 1930'ies. During the first decades, production mainly came from eluvial and alluvial workings, but progressively exploitation was oriented underground by selectively mining the quartz veins. Cumulative production from different deposits in the Rutongo area reached ~30000 tons of cassiterite between 1931 and 1982. Currently, the possibilities for (semi-) industrial mining are being evaluated again. Secondary deposits are considered to be exhausted, but – mainly primary – resources are estimated at ~6700 tons of certain resource, ~10700 tons of probable resource and ~6900 tons of possible resource (unpublished data Société Minière du Rwanda [SOMIRWA]).

Although many historical (pre-independence DRC & Rwanda-Burundi) mineralogical and general geological studies are reported on the mineralisation in the Kibara orogen (e.g. Agassiz, 1954; De Kun, 1954, 1959; Legraye, 1955; Peeters, 1956; Safiannikoff, 1955; Steenstra, 1967; Varlamoff, 1948, 1950, 1954a,b,c, 1956, 1961, 1963, 1969, 1975), only few recent metallogenic studies have been carried out to explain the formation and origin of the mineralisation, using modern laboratory techniques and metallogenic models of granite-related rare element ore-deposits (Günther, 1990; Pohl, 1994; Pohl & Günther, 1991; Dewaele et al., 2007a, 2007b, 2008, accepted; De Clercq et al., 2008).

This article combines "historical" information (i.e. mining archives of the former Belgian colonial and post-colonial mining companies: Société Minière de Muhinga et de Kigali (SOMUKI) and Société des Mines du Rwanda (SOMIRWA)), with selective new data and analyses to obtain an updated metallogenic model for the formation of the vein-type cassiterite mineralisation in the Mesoproterozoic Kibara orogen. The main quarries in the Rutongo area were visited to control the "historical" geological data and to sample new material. It should be noted that the mines have not been exploited in an organised way since mid 80'ies, which complicated underground observations.

2. Geological Setting

2.1 Geology of the Kibara orogen

The Kibara orogen formed and evolved between two pre-Mesoproterozoic domains: the Archaean-Palaeoproterozoic Congo craton to the west and the north, and the Archaean- and Palaeoproterozoic Tanzania craton and Bangweulu Block to the east and the south. The Kibara belt consists of two distinct segments, separated in the Kivu area of the Democratic Republic of the Congo (DRC) by the northwestern extension of the Palaeoproterozoic Ubende belt (SW Tanzania) across Lake Tanganyika. The "Northern" (Rwanda, Burundi, Maniema and Kivu in the DRC) and "Southern" (Katanga in the DRC) segments should be viewed as two separate – albeit coeval – orogenic belts (Tack et al., 2002a, 2002b,

2006). Numerous models exist concerning the origin of the Mesoproterozoic Kibara belt. It has been interpreted as a collisional orogeny (Kampunzu et al., 1986, Rumvegeri, 1991), as an intracratonic orogen with different periods of extension and compression (Klerkx et al., 1984, 1987), and as an intracratonic extensional detachment structure, conditioned by strike-slip reactivation of NW-trending shear zones in the Palaeoproterozoic basement (Fernandez-Alonso & Theunissen, 1998).

The Kibara orogen consists dominantly of Palaeo- and Mesoproterozoic rocks that were intruded by different generations of granites (Fig. 1; e.g. Cahen et al., 1984). These were identified based on petrographic observations and Rb-Sr dating (Cahen et al., 1984). However, recent U-Pb Shrimp dating indicates the presence of only two main granite generations in the Kibara orogen (Kokonyangi et al. 2004; 2006; Tack et al., 2006, 2008). In the northern part of the Kibara orogen (Kivu, Rwanda and Burundi), the main granite generation G1-3 intruded the Palaeo- and Mesoproterozoic rocks at 1380 ± 10 Ma (U-Pb SHRIMP zircon; Tack et al., 2006, 2008). The crystallisation of these granites did not result in an economically significant concentration of rare metals (Dewaele et al., accepted). At 986 ± 10 Ma, the so-called Kibara G4-granites or "tin granites" were emplaced (U-Pb SHRIMP zircon; Tack et al., 2006; 2008). Their intrusion is attributed to the ~ 1.0 Ga main compressional regime, which resulted in the preferential development of syn-form upright folding of the metasediments and S_2 cleavage (Tack et al., 2006; 2008). This compressional event has been interpreted as an intraplate far-field effect related to the 1.0 Ga "global" collisional orogeny that led to Supercontinent Rodinia amalgamation at the end of the Mesoproterozoic Era (Tack et al., 2002a; 2002b; 2006; 2008). Regional metamorphism is in general low grade, while higher grades are confined to tectono-metamorphic complexes or in the vicinity of granitic domes (Gérards & Ledent, 1970; Fernandez-Alonso & Theunissen, 1998). After intrusion of the G4-granites, pegmatites were emplaced at 968 ± 8 Ma (Brinckmann & Lehmann, 1983). Columbite-tantalite and cassiterite mineralisation are associated with some of these pegmatites. The columbite-tantalite mineralisation has been dated in Burundi at 965 ± 5 Ma and 962 ± 2 Ma (Romer & Lehmann, 1995; Brinckmann et al., 2001), which overlaps with the timing of pegmatite emplacement. The entire set has been cut by quartz veins that have been dated at 951 ± 18 Ma (Rb-Sr muscovite, Brinckmann et al., 1994). These quartz veins may contain cassiterite and/or wolframite mineralisation.

2.2 Geology of the Rutongo area

Detailed geological information on the Rutongo area and – more specific – on the individual mining sites is available in the archives of the Royal Museum for Central Africa (RMCA, Tervuren) and originates from the former colonial and post-colonial Belgian mining companies (mainly SOMUKI and SOMIRWA) that were active in the area. More recently, the mineralisation in the Rutongo area has been studied by Günther (1990), Pohl & Günther (1991), Pohl (1994) and Dewaele et al. (2007b).

The Rutongo area is situated on an important anticline (Fig. 2), the so-called Rutongo anticline, adjacent to the Yanza syncline in the W and the Nzoko-Rwamahili syncline in the E (Bertossa et al, 1964; Pohl, 1975). The Rutongo anticlinal structure plunges to the north and has a westward vergency. In the eastern part of the anticline, the dip of the bedding planes is ~15°, while it attains about 60-70° in the western part. Different thrust faults have

Group	Formation	Reference sandstone unit	Intermediate package	Thickness (m)
Pindura	Bulimbi			
Gikoro	Nduba	Nduba quartzite		30
	Musha		Quartzophyllites	500
	Nyabugogo	Kyanza sandstone		50
			Phyllites and small sandstones	250
		Mahaza quartzite		95
			Phyllites and small sandstones	300
		Karambo sandstone		120
			Phyllites	350
		Kisanze quartzite		170
			Phyllites	150
		Hôpital quartzite		50
			Phyllites	250
		Kitaba sandstone		50
			Phyllites	150
		Rutongo-Gasambya quartzite		130
			Phyllites	180
		Masoro quartzite		30
			Phyllites and small sandstones	200
		Mugambazi sandstone		100
			Kambo phyllites and sandstone bancs	465

Table 1. Updated geological stratigraphic column, showing a combination of the historical different quartzite units (column reference quartzite unit and intermediate package) in the Rutongo area (cf Lhoest 1957b; Pohl, 1975) and the recent stratigraphy of Baudet et al. (1988) (column Group and Formation).

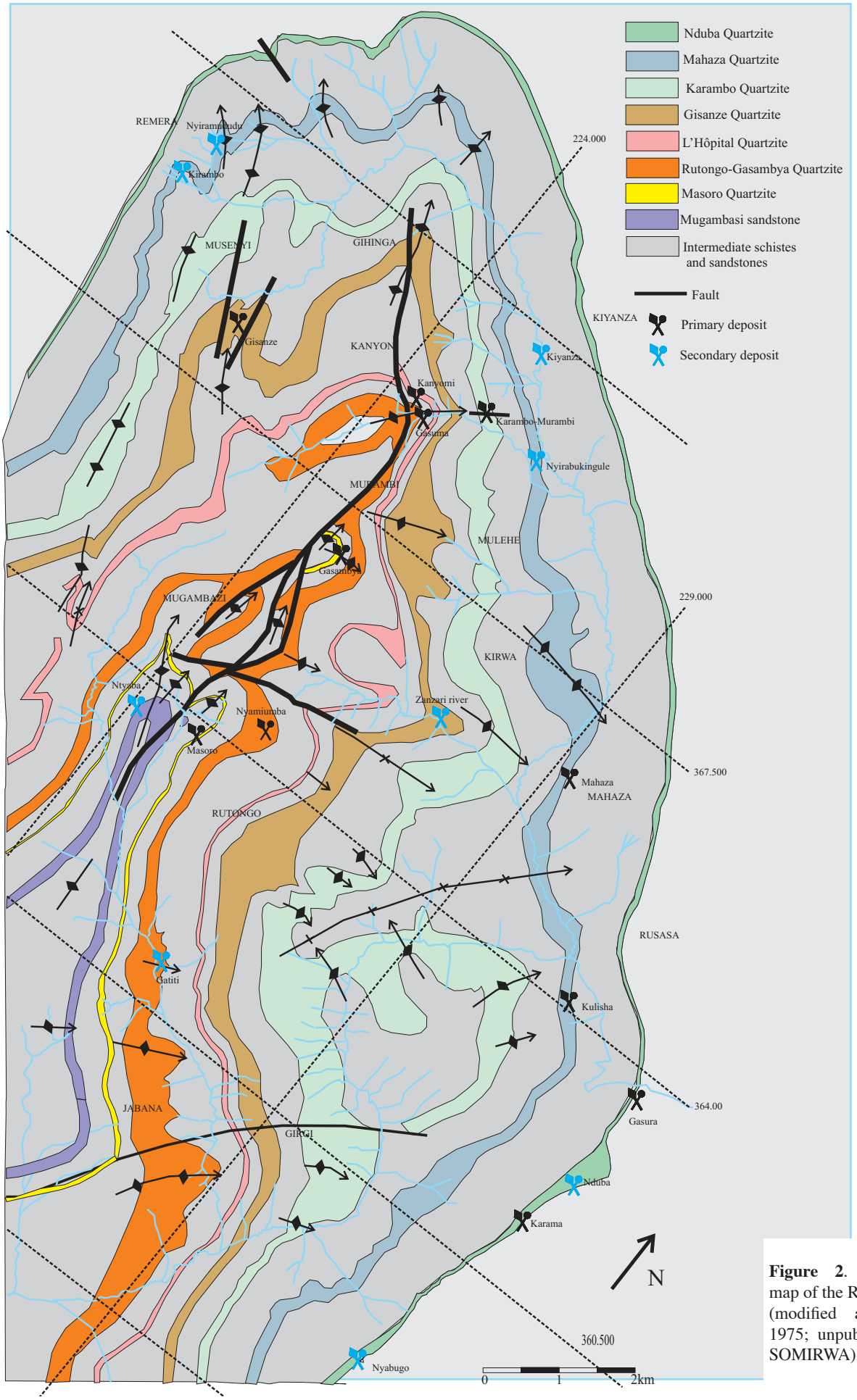

Figure 2. Geological map of the Rutongo area (modified after Pohl, 1975; unpublished data SOMIRWA).

been mapped in the main anticline: NS oriented low-angle thrust faults in the centre and EW oriented faults in the southern part (Peeters, 1956; Lhoest, 1957a, b; Pohl, 1975). Two fold orientations have been identified. The first is oriented N-S and runs parallel to the main axis of the anticline, while the second is E-W. The dip of the E-W axes is not large, but increases towards the centre of the anticline (up to 50°). The N-S oriented folds are mostly developed in the core and in the western part of the anticline. The transversal E-W orientations mostly developed in the eastern part of the anticline.

The Mesoproterozoic rocks found in the Rutongo area belong to the lower and middle part of the Rwanda Supergroup (Gikoro and Pindura Group) (Baudet et al., 1988). They typically consist of a succession of different low grade metamorphosed quartzite units, separated by large packages of metapelites with intercalations of quartzite. The rocks in the Rutongo area have only been submitted to a regional low grade metamorphism (Baudet et al., 1988). Detailed mapping of Lhoest (1958) and Pohl (1974; 1975; unpublished data SOMIRWA) resulted in a detailed stratigraphy and geological map of the Rutongo area (Table 1 and Fig. 2), during which 9 main quartzite units have been identified. An important observation of Pohl (1974, 1975) is that the quartzite units are not continuous for tens of kilometres but rather can be interpreted as lenticular bodies. The presence of conglomerates, quartzites with ripple marks, the alternation of metapelites and quartzites and cross-laminated beds, etc. allowed Baudet et al. (1988) to postulate a sedimentation environment close to the coast, more specifically of turbiditic and deltaic deposits. These depositional environments are complex and cause important lateral variations. Cleavage planes can be observed in the metapelitic host rocks. According to Lhoest (1957a), their orientation is more or less parallel, but their inclination varies. At the scale of the anticline, the inclination is fan-shaped, i.e. dipping to the east in the eastern flank and to the west in the western flank (Lhoest, 1957a). However, in the Sn-mineralised areas in the centre of the anticline, the cleavage planes are weakly expressed and are only locally present (Lhoest, 1957a; Pohl, 1975).

In the south-eastern part of the Rutongo anticline, granitic rocks of the Kigali granite can be found on the left bank of the Nyabugogo river. The Kigali granite has intrusive contacts with the quartzite units. The Kigali granite is generally strongly kaolinised and sericitised, but some fresh parts identify it as a two-mica granite (Bertossa et al., 1964). In the contact zone between the granite intrusion and the host-rocks, it can be seen that the intrusion postdates microfolds in the host-rocks (Lhoest, 1957a, b). The Kigali granite is interpreted to have been emplaced during a late phase or post-folding of the rocks, when the latter already had formed the general style of the layers (Peeters, 1956; Lhoest, 1957a, b; Bertossa et al., 1964, Pohl, 1974). Peeters (1956) observed on a microscopic scale minor crushing of the granites, with resulting mechanical deformation and recrystallisation of feldspar crystals. According to the author, this is an indication of a second tectonic phase, less important than the first that took place after intrusion of the granites. In the contact zone between the granite and the host-rock, the rocks are impregnated with tourmaline crystals, which crosscut the microfolds (Lhoest, 1957a, b). Also, some small scale muscovite-tourmaline bearing pegmatites occur in the contact zone (Lhoest, 1957a). The Kigali granite has been interpreted to belong to the youngest granite generations of the Kibara orogen (G4-granite) (Pohl, 1975). Lhoest (1957a, b) and Pohl (1975) described in the eastern part of the Rutongo anticline different anticlinal domes caused by granite intrusion. The most remarkable domes are the Nyabugogo dome, situated on

Prefecture	Commune	Name deposit	Geological formation	Minerals		Type of mineralisation		Geographical location	
				SnO_2	WO_3	Q-vein	detrital	coX	coY
Kigali	Mbogo	Ntaba	Nyabugogo formation	x			x	1°44'	29°59'
		Nyiramududu	Musha formation	x			x	1°45'	30°01'
		Kirambo (Lusine amont)	Musha formation	x			x	1°46'	30°00'
		Mbogo (Mulindi Source)	Musha formation		x		x	1°46'	29°59'
	Mugambazi	Gisanze	Nyabugogo formation	x		x		1°47'	30°01'
		Kanyoni	Nyabugogo formation	x		x		1°47'	30°01'
		Gasuma (Nyakibande)	Nyabugogo formation	x		x		1°47'	30°03'
		Kiyanza	Musha formation	x			x	1°46'	30°03'
		Nyamuko	Bulimbi formation	x			x	1°45'	30°04'
		Karambo-Murambi	Nyabugogo formation	x		x	x	1°46'	30°03'
		Muyanza (Aval)	Bulimbi formation	x			x	1°46'	30°05'
		Nyirabukingure	Nyabugogo formation	x			x	1°46'	30°04'
		Gasambya	Nyabugogo formation	x		x	x	1°48'	30°03'
		Zanzari riv	Nyabugogo formation	x			x	1°48'	30°04'
		Mahaza	Nyabugogo formation	x		x	x	1°48'	30°05'
		Ntyaba	Nyabugogo formation	x			x	1°48'	30°02'
		Gatiti (riv Mulindi)	Nyabugogo formation	x			x	1°51'	30°07'
		Gatare (Rusasa-Nord)	Bulimbi formation	x			x	1°49'	30°07'
		Rusasa	Nyabugogo formation	x			x	1°49'	30°07'
	Gikomero	Kulisha I en II	Nyabugogo formation	x		x	x	1°49'	30°06'
		Gasura	Bulimbi formation	x		x		1°50'	30°07'
		Nduba	Bulimbi formation	x			x	1°50'	30°07'
		Karama	Nyabugogo formation	x		x	x	1°51'	30°60'
		Nyabugo	Nyabugogo formation	x			x	1°51'	30°06'
	Rutongo	Nyamyumba (Rutongo)	Nyabugogo formation	x		x	x	1°49'	30°03'
		Masoro (Mugambazi et Kigoma)	Nyabugogo formation	x		x	x	1°50'	30°03'
		Karuruma	Nyabugogo formation	x			x	1°53'	30°03'

Table 2. Summary table showing the different mineralisation that have been reported in the Rutongo area (information from archives RMCA), with indication of type of mineralisation and the coordinates.

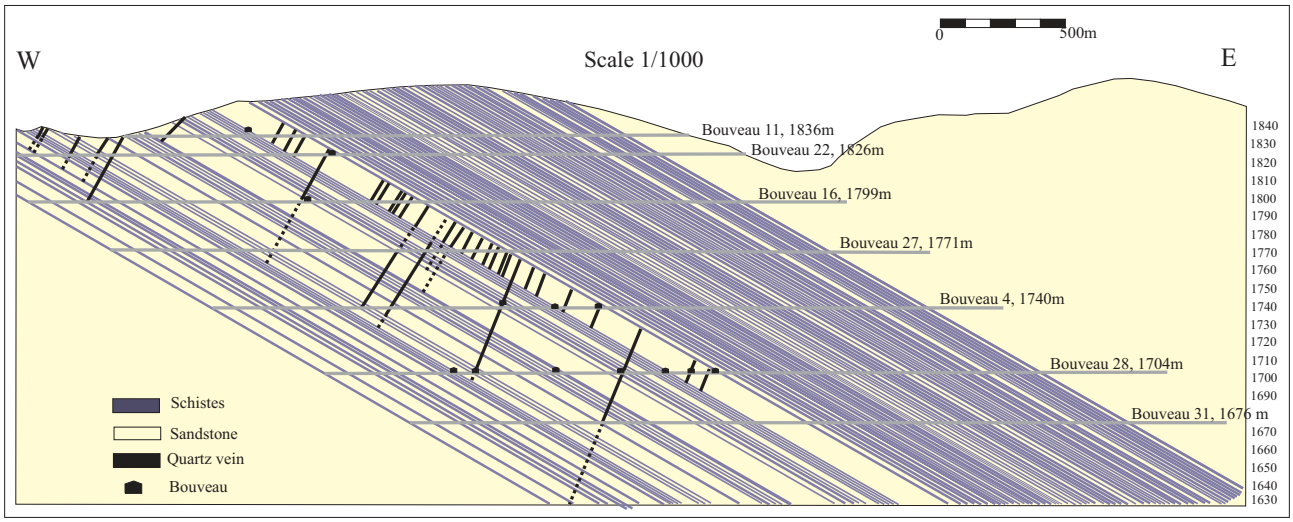

Figure 3.Cross-section through the axis of secondary anticline at Nyamiumba (modified after unpublished data of SOMIRWA), with indication of different drives (bouveaus). A to M refers to a certain quartzite level.

the left bank of the Nyabugogo river, and the Nyirabukingule dome, situated south of Kanyoni.

2.3 Cassiterite mineralisation in the Rutongo area

An overview (Table 2) of the different mineral occurrences in the Rutongo area was compiled from the information in the mining archives of the RMCA. The area is mainly characterised by cassiterite mineralisation (26 of 27 deposits). For one deposit (Mulindi Source), tungsten mineralisation has been described. Most of the deposits are secondary alluvial (23 of 27 deposits), while only 11 primary quartz vein mineral occurrences are known. Some occurrences contain primary quartz veins as well as secondary alluvial deposits. The majority of quartz vein deposits have been described for the Nyabugogo Formation (10 of 11 deposits), which is also the case for the secondary deposits (15 of 23 deposits). The individual vein systems occur, however, in different quartzite units. The most important primary mineralisation can be found at Nyamiumba, Gasambya, Karambo, Murambi, Masoro and Mahaza, all located in the eastern flank of the anticline. Using aerial photographs and unpublished geological maps of the former SOMIRWA, all primary mineralisation could be linked to a lineament that has been interpreted as a fault (see Fig. 2).

The primary mineralisation in the Rutongo area consists of mineralised quartz veins that often occur in sub-parallel swarms. Several hundreds of quartz veins can be found. The quartz veins are generally restricted to the quartzite units (Fig. 3). Only a limited number of veins cut the metapelitic rocks, situated between the quartzite bancs. The average width of the veins varies between 0.5 and 1m, with minimum and maximum width of some centimetre up to several meters respectively. The extension of the quartz veins can vary significantly, but is mostly determined by the thickness of the quartzite units. The quartz veins can have an extension of some meters up to several hundreds of meters. In the economically most important mineralisation (Nyamiumba, Masoro, Gasambya, Karambo, Murambi and Mahaza), the veins are oriented NS, with a dip of 60° to the west (unpublished archives SOMIRWA; Lhoest, 1957a; Pohl, 1975). The quartz veins can be crosscut by less thick and less regular quartz veins. The lower part of the mineralized quartz veins is particularly rich in cassiterite (Aderca, 1957; Lhoest, 1957a).

3. Petrography and paragenesis

The paragenetic sequence (Fig. 4) of the cassiterite mineralisation in the Rutongo area has been studied on samples from different quartz vein occurrences, i.e. Masoro, Mahaza and Nyamiumba (Fig. 2). Thin and polished sections have been studied by transmitted and incident light microscopy.

In the Rutongo area, the host-rock of the mineralised quartz veins is dominantly composed of quartzite, with smaller intercalations of metapelitic rocks. The quartzites are very pure and contain only a limited amount of additional minerals (mainly feldspars, detrital muscovite and biotite and sulphides) in addition to quartz. The quartz grains are intensely compacted and recrystallized due to a low grade regional metamorphism. The quartz veins are bordered with a dark rim of tourmaline (Plate 1C), which passes into more disseminated tourmaline and muscovite (Plate 2A, B) further away from the vein. This zonation in alteration is caused by sericitisation, silicification, tourmalinisation and muscovitisation. The quartzites often show a slight cleavage development. Tourmaline and muscovite crystals can be found along this foliation orientation (Plate 1A, 2C). In addition, it can be observed in some samples that the quartz veins, with associated alteration, crosscut the foliation. This would imply a syn- to post-cleavage development of the alteration and quartz

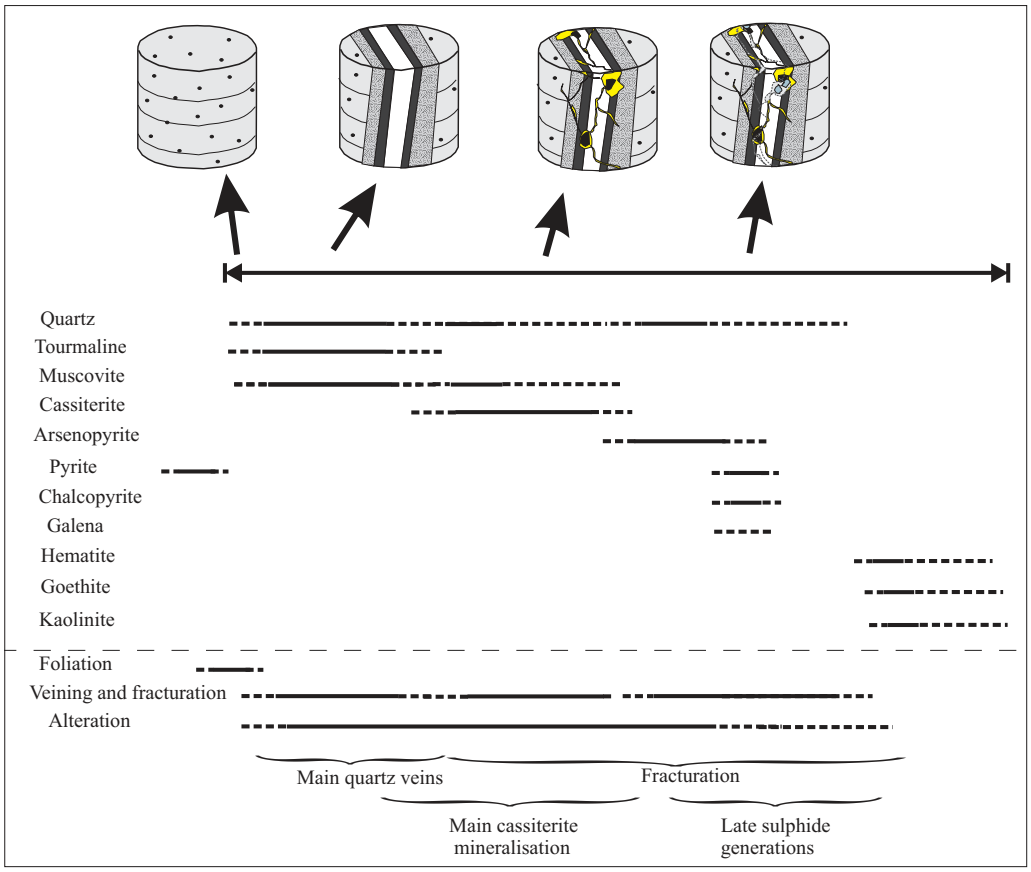

Figure 4. Paragenesis of the Rutongo mineralisation.

veins. Intercalated metapelitic layers in the quartzite units are often completely altered to tourmaline (the so-called "tourmalinite" rocks).

The quartz vein itself is fractured. The fractures are dominantly filled with muscovite, associated with minor quartz. Cassiterite mineralisation is concentrated in certain zones of these fractures and associated with large muscovite crystals (i.e. the so-called "poches de greisen", Plate 1B, 2D). The mineralisation is mostly present in the centre or at the margin of the quartz veins. The cassiterite crystals show a colour zonation (Plate 2E) and are often recrystallised and fractured. The fractures are filled with arsenopyrite (Plate 2F), pyrite, chalcopyrite and galena associated with another quartz generation. Recent weathering resulted in the formation of hematite, goethite and kaolinite in fractures.

4. Stable isotopes

$\delta^{18}O$ and δD stable isotope analysis of quartz and cassiterite from mineralised quartz veins has been carried out at the SUERC in East Kilbride, Scotland. Quartz samples were selected based on their relationship with the mineralisation and hand-picked. All separates were analysed for $\delta^{18}O$ using a laser fluorination procedure, involving total sample reaction with excess ClF_3 using a CO_2 laser as a heat source. Reproducibility is around 0.3‰ (1σ). Results were reported as per mil (‰) deviations from the Vienna Standard Mean Ocean Water (V-SMOW) standard. Samples of quartz and cassiterite were selected for measurement of inclusion fluid δD. Although handpicking ensured that mineral separates were pure, it was unavoidable that different fluid generations were sampled (cf. Günther, 1990; Dewaele et al., 2007b). In the quartz and cassiterite samples, no primary inclusions were found along crystal growth zones. In the cassiterite crystals, the fluid inclusion population is dominated by randomly dispersed inclusions that have been interpreted as ambient fluids responsible for cassiterite precipitation, whilst the quartz crystals are dominated by secondary fluid inclusions (Dewaele et al., 2007b). The technique involves decrepitation of fluid inclusion under vacuum using bulk samples (> 600 mg quartz) following the technique of Fallick et al. (1987). Data are reported in δD notation as per mil (‰) variations from Vienna Standard Mean Ocean Water (V-SMOW). Reproducibility of this procedure is around 5‰.

Location	Mineral	$\delta^{18}O$	δD	
Nyamiumba	Quartz	14	-29.9	*
Nyamiumba	Quartz	13.5		*
Mahaza	Quartz	15	-65	
Musha	Quartz	15.3	-40	
Nyamiumba	cassiterite	6.6		*
Nyamiumba	cassiterite	5.5	-95	
Musha	cassiterite	6.2	-76	

Table 3. Uncorrected $\delta^{18}O$-δD data from quartz of mineralised veins of Rutongo, Mahaza and Musha and from cassiterite of Musha and Nyamyumba. * from Dewaele et al. (2007b).

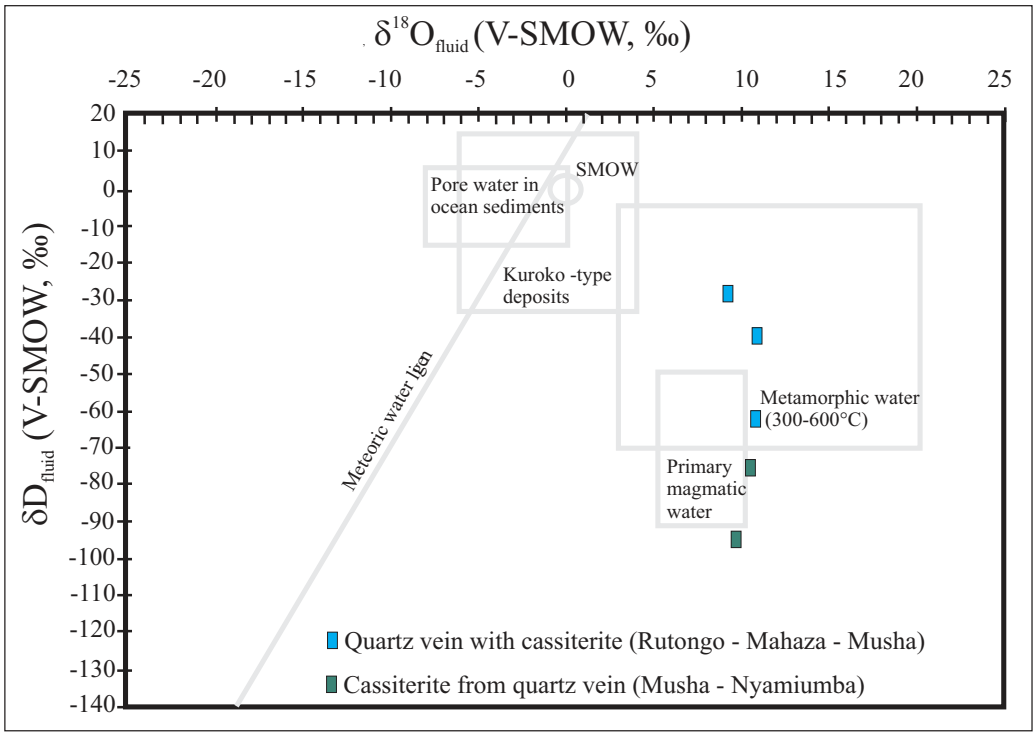

Figure 5. $\delta^{18}O$-δD isotopic plot for the calculated fluid composition (400°C) of the mineralised quartz veins of Nyamiumba, Mahaza and Musha and of cassiterite from Musha and Nyamiumba. The meteoric water line, the isotopic fields of metamorphic and of primary magmatic fluids and of volcanic-associated massif sulphide (Kuroko type) deposits are drawn after Yurtsever & Gat (1981), Pisutha-Arnond & Ohmoto (1983), Ohmoto (1986) and Sheppard (1986).

Four quartz samples (Nyamiumba, Mahaza and Musha) and three cassiterite samples (Nyamiumba and Musha) from mineralised quartz veins were selected to trace the origin of the mineralising fluids (Table 3). Musha is a similar vein-type cassiterite mineralisation as those in the Rutongo area, but located 40 km to the east (Fig. 1). The $\delta^{18}O$ value of the ambient fluids responsible for the precipitation of cassiterite and quartz is calculated based on a pressure corrected Th_{Tot} of the fluid inclusions (~400°C; Günther, 1990). The calculated oxygen isotopic compositions of the ambient fluid show marked similarity between the fluids involved in depositing cassiterite and quartz, ranging between +9 ‰ and +10.8 ‰ V-SMOW for quartz and between +9.6 ‰ and +10.4 ‰ V-SMOW for cassiterite. The δD values vary between -29.9 ‰ to -65 ‰ V-SMOW for quartz and between -76 ‰ and -95 ‰ V-SMOW for cassiterite.

The formation temperature of the cassiterite, calculated based on the isotopic equilibrium between cassiterite and quartz from Nyamiumba and Musha is ~ 400°C, which is comparable to the pressure-corrected temperature obtained by fluid inclusion microthermometry (Günther, 1990). Thus, equilibrium seems to have been established between the two phases. However, in a $\delta^{18}O$-δD plot, the values for the quartz samples plot in the field typical for metamorphic fluids whereas the cassiterite samples plot slightly to the right and below of the field typical for primary magmatic fluids, definitely outside of the field for metamorphic fluids (Fig. 5).

5. Lead isotopes

Lead isotope analyses were carried out on sulphides from the mineralisation and the host-rock using Thermal

Sample	Location	Origin		$^{206}Pb/^{204}Pb$	$^{207}Pb/^{204}Pb$	$^{208}Pb/^{204}Pb$	
9347	Ruhengeri	Sed		**18.39**	**15.73**	**39.3**	*
9348	Ruhengeri	Sed		**18.69**	**15.76**	**39.19**	*
9372	Nyungwe	Sed		**18.77**	**15.76**	**39.19**	*
9378	Shari	Sed		**18.84**	**15.76**	**38.63**	*
9373	Gatumba	Peg		**25.45**	**16.25**	**41.83**	*
9376	Rwansibo	Peg		**18.65**	**15.74**	**38.43**	*
25	Shyorongi	Q + W		**18.64**	**15.74**	**38.97**	*
26	Shyorongi	Q + W		**18.25**	**15.69**	**37.85**	*
6005	Rutongo	Q + Sn		**18.26**	**16.1**	**38.4**	**
6006	Rutongo	Q + Sn		**18.76**	**16.15**	**38.98**	**
RG 8539	Rutongo-Kigali	Sed	Py	**18.580**	**15.898**	**38.511**	
RG 10281	Concentrate Rutongo	Q + Sn	Asp	**18.846**	**15.998**	**39.199**	
RG 10281	Concentrate Rutongo	Q + Sn	Py	**18.615**	**15.950**	**38.676**	
RG 6006	Rutongo-Kababara	Q + Sn	Gn	**18.156**	**15.942**	**37.951**	
RG 6005	Rutongo-Karambo	Q + Sn	Gn	**18.118**	**15.892**	**37.793**	
RG 9633	Kirengo	Peg	Py	**18.251**	**15.910**	**37.906**	
RG 9981	Buranga	Peg	Py	**27.072**	**16.512**	**40.889**	

Table 4. Existing and new Pb/Pb data of sulphides related to mineralisation in Rwanda. * from Cauet & Pohl (1988); ** from Monteyne-Poulaert et al. (1962). Analysis of RG samples are from Dewaele et al. (2008)

Ionization Mass Spectrometry (TIMS). Samples were weighted and dissolved in 8M HBr. After evaporation to dryness, residues were dissolved in nitric acid, dried again and dissolved in 1 ml of deionised water. Sample aliquots of roughly 250 ng Pb were loaded on single Re filaments using silica gel and dilute phosphoric acid. The isotopic composition was measured on a six collector Finnigan MAT 261 mass spectrometer running in static multicollection mode. Pb isotope ratios were corrected for instrumental mass fractionation using a discrimination factor of 0.123 ± 0.029 % per amu (2σ) based on replicate analysis of the NBS SRM 981 Pb standard. Errors and error corrections were calculated according to Ludwig (2003). The 2σ uncertainties amount to 0.06, 0.09 and 0.12 % for the $^{206}Pb/^{204}Pb$, $^{207}Pb/^{204}Pb$ and $^{208}Pb/^{204}Pb$ ratios, respectively.

Pb/Pb analyses have mainly been carried out on sulphides of the sulphide mineralisation stage of the paragenesis (Table 4), which postdates the main cassiterite mineralisation in the paragenesis (Dewaele et al., 2008). The data obtained is comparable with the values from older literature (Monteyne-Poulaert et al., 1962a; Cauet & Pohl, 1988). It has been observed that the values cluster with the values from dispersed pyrite from the surrounding rocks. This could indicate that the Pb originates from the surrounding sedimentary rocks (cf. Pohl & Günther, 1991; Pohl, 1994).

6. Ar-Ar dating

Muscovite crystals associated with cassiterite mineralisation in a fracture in a larger quartz vein from Nyamiumba were analyzed by the Ar–Ar stepheating technique. The mineral fractions were hand-picked under a binocular microscope. The separates were weighted, wrapped in Al foil and were vacuum-encapsulated in quartz vials with the neutron flux monitor Hb3gr (t = 1073.6 ± 5.3 Ma; Jourdan et al., 2006). Nuclear irradiation was carried out on position B2W of the SAFARI-1 reactor at Pelindaba, South Africa, using a fast neutron flux of ~2×10^{18} n cm^2. The J value determined from Hb3gr was 0.01034 ± 0.00010 (2σ).

The Ar isotopes were measured using an MS1 mass spectrometer at the University of Manchester, equipped with a Baur-Signer ion source and a Faraday collector. The irradiated samples were step-heated in a Ta-resistance furnace over the temperature interval of 500 to 1600 °C, using 30 min heating steps. During heating, Ar was purified using a Zr–Al getter at 450 °C. Raw isotopic data were corrected for mass discrimination (calibrated using atmospheric argon), radioactive decay and neutron interference corrections. Further experimental details are given by Burgess et al. (2004). $^{40}Ar–^{39}Ar$ ages were determined from age spectrum diagrams, using the ISOPLOT/Ex 3.23 software (Ludwig, 2003), and all data are reported at the 2 σ level of uncertainty. The isotopic data are given in Table 5 and age spectrum diagram is plotted in Fig. 6.

Temp. (ºC)	^{36}Ar ($\times 10^{15}$ moles)	Cl^1 ($\times 10^{9}$ moles)	Ca^2 ($\times 10^{9}$ moles)	K^3 ($\times 10^{9}$ moles)	^{40}Ar ($\times 10^{15}$ moles)	$^{40}Ar^{*4}$ (%)	Cum. ^{39}Ar (%)	$^{40}Ar^*/^{39}Ar$	Age^5 (Ma)
SD05	mass = 0.01099 g								
700	0.29 ± 0.13	0.4 ± 0.06	32.9 ± 26.9	46.3 ± 0.6	322.1 ± 0.6	73.1	0.3	40.2 ± 6.4	627.2 ± 83.9
800	0.46 ± 0.09	0.28 ± 0.04	58.8 ± 40.4	308.0 ± 3.0	1802.8 ± 2.3	92.5	2.5	42.8 ± 0.7	661.0 ± 8.4
900	0.22 ± 0.14	nd	154.8 ± 153.0	4617.5 ± 44.1	36341.8 ± 63.1	99.8	34.7	62.1 ± 0.1	894.9 ± 1.3
930	0.13 ± 0.14	nd	46.8 ± 85.3	1820.2 ± 17.5	14098.7 ± 18.8	99.7	47.4	61.1 ± 0.2	883.0 ± 2.3
950	0.28 ± 0.09	0.23 ± 0.14	133.4 ± 58.0	725.4 ± 7.5	5514.5 ± 8.0	98.5	52.5	59.2 ± 0.4	861.3 ± 4.5
980	3.06 ± 0.07	0.15 ± 0.04	173.0 ± 38.2	778.8 ± 7.5	6617.2 ± 10.2	86.3	57.9	58.0 ± 0.2	847.6 ± 2.6
1000	0.32 ± 0.09	0.13 ± 0.07	149.8 ± 35.2	759.3 ± 7.3	5734.5 ± 9.0	98.3	63.2	58.7 ± 0.3	855.8 ± 3.2
1020	0.23 ± 0.09	0.11 ± 0.06	171.2 ± 34.4	851.5 ± 8.2	6373.1 ± 11.4	99.0	69.2	58.6 ± 0.3	854.0 ± 3.0
1040	0.32 ± 0.09	0.34 ± 0.09	200.9 ± 47.6	997.2 ± 9.6	7411.7 ± 10.4	98.7	76.1	58.0 ± 0.2	847.7 ± 2.6
1060	0.34 ± 0.09	0.42 ± 0.14	232.3 ± 45.8	1407.1 ± 13.6	10512.8 ± 13.8	99.0	85.9	58.5 ± 0.2	853.4 ± 2.1
1080	0.33 ± 0.10	0.34 ± 0.07	219.5 ± 52.1	1052.2 ± 10.1	7911.9 ± 11.2	98.8	93.3	58.7 ± 0.2	856.0 ± 2.7
1100	0.40 ± 0.09	0.15 ± 0.04	145.3 ± 40.4	576.9 ± 5.6	4243.2 ± 5.6	97.2	97.3	56.5 ± 0.4	830.4 ± 4.5
1150	0.40 ± 0.06	0.09 ± 0.03	83.9 ± 40.9	288.7 ± 2.8	2156.1 ± 3.0	94.5	99.3	55.8 ± 0.5	821.4 ± 5.5
1300	1.07 ± 0.08	0.03 ± 0.05	56.4 ± 20.7	68.1 ± 0.7	762.1 ± 1.1	58.7	99.8	51.9 ± 2.7	775.3 ± 32.9
1500	3.09 ± 0.06	0.02 ± 0.05	12.8 ± 12.8	28.3 ± 0.4	1082.1 ± 1.5	15.5	100.0	46.9 ± 5.0	713.3 ± 63.0
Total	*10.94 ± 0.37*	*1.67 ± 0.41*	*1871.7 ± 226.4*	*14325.5 ± 54.0*	*110884.3 ± 72.0*			*59.4 ± 0.1*	*863.9 ± 6.6*

[1] Determined from $^{37}Cl(n,\gamma,\beta)^{38}Ar$: $Cl = 9.0159\times10^{4}.\frac{^{38}Ar}{\beta\cdot J}\cdot(\text{mole/mole})$; $\beta = \left(\frac{K}{Cl}\cdot\frac{^{38}Ar}{^{39}Ar}\right)_{Hb3gr}$; $(K/Cl)_{Hb\,3gr} = 5.242$; $\beta = 7.13 \pm 0.07$

[2] Determined from $^{40}Ca(n,\alpha)^{37}Ar$: $Ca = 8.042\times10^{4}.\frac{^{37}Ar}{\alpha\cdot J}\cdot(\text{mole/mole})$; $\alpha = \left(\frac{K}{Ca}\cdot\frac{^{37}Ar}{^{39}Ar}\right)_{Hb3gr}$; $(K/Ca)_{Hb\,3gr} = 0.1674$; $\alpha = 0.505 \pm 0.001$

[3] Determined from $^{39}K(n,p)^{39}Ar$: $K = \frac{^{39}Ar}{J}\cdot\frac{K}{^{40}K}\cdot\frac{\lambda}{\lambda_e}$ (mole/mole); $\lambda/\lambda_e = 0.581$; $K/^{40}K = 1.167\times10^{-4}$; $J = 0.01035\pm0.000027$

[4] $^{40}Ar^* = {}^{40}Ar_{total} - 295.5\times{}^{36}Ar$

[5] Includes uncertainties on the J value.

Table 5. ^{40}Ar-^{39}Ar analytical data for a muscovite sample from Nyamiumba (SD05).

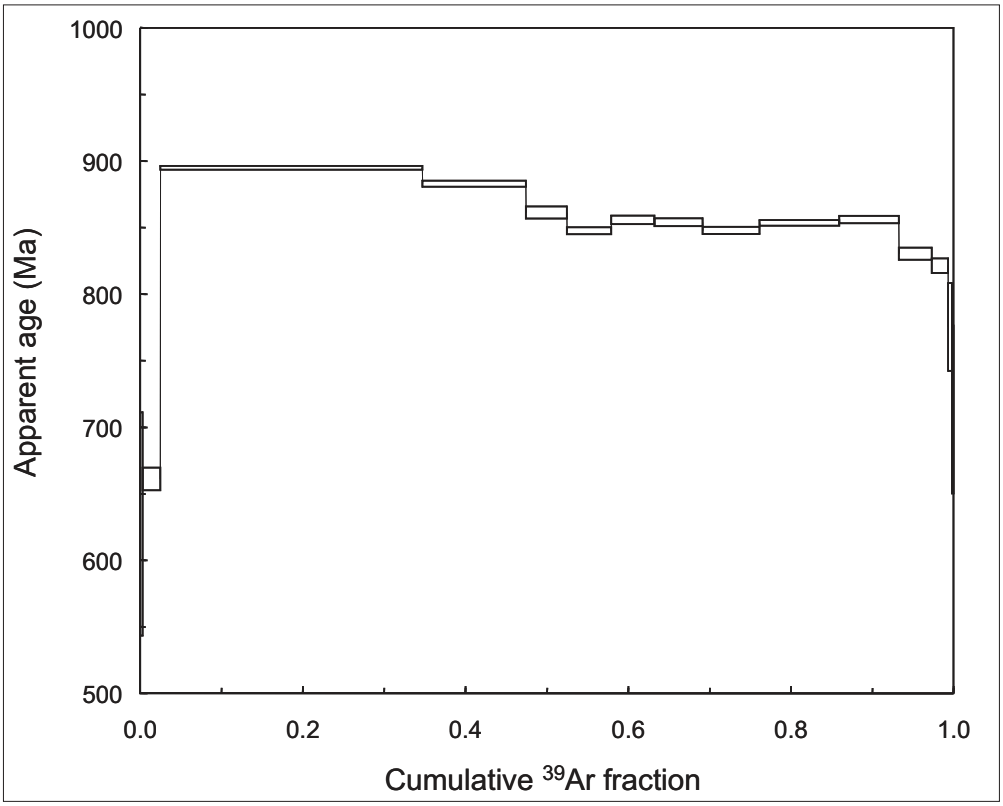

Figure 6. ^{40}Ar-^{39}Ar spectrum of muscovite from Nyamiumba.

The Nyamiumba muscovite sample shows low apparent ages in the first two steps, followed by a maximum age step at 900°C of 895 Ma comprising 32% of the ^{39}Ar release. Apparent ages then decline to 848 Ma at intermediate release before rising again to 869 Ma, followed by a further decrease at higher temperature. The integrated age of the sample, excluding the two low temperature steps, is 869 ± 7 Ma (2σ including uncertainties on the J value). Overall the apparent age spectrum is upwards-convex (Wijbrans and McDougall, 1986), a relatively common shape for micas (phengite, muscovite and biotite) from orogenic terrains. This type of spectrum is not readily interpreted using the concept of plateau age (i.e. single diffusion domain) and may relate to Ar degassing from two or more different microstructural or microchemical domains or mixed mica phases (e.g. Forster and Lister, 2004). Data do not define an isochron on a plot of $^{36}Ar/^{40}Ar$ versus $^{39}Ar/^{40}Ar$, but does indicate that any non-radiogenic Ar in the sample is most likely to be atmospheric argon.

Despite the lack in understanding the details of the apparent age variations during stepped heating of Nyamyumba muscovite, the range of ages obtained (895-869 Ma) is clearly younger than the ages obtained for the G4-granite (986 ± 10 Ma, Tack et al. 2006, 2008), for the Kibara pegmatites (968 ± 8 Ma, Brinckmann et al. 2001), with associated columbite-tantalite mineralisation (965 ± 5 Ma; Romer & Lehmann 1995) and also for the quartz vein of Mulehe in Burundi (951 ± 18 Ma; Brinckmann et al., 1994). Our present lack of detailed understanding of the apparent age variations in our sample of Nyamyumba muscovites would lead us to an integrated age of 869 ± 7 Ma, with a possible upper limit of ~ 895 Ma. The possible geological significance of this age is discussed below.

7. Discussion and conclusion

7.1 Source of cassiterite mineralisation in Rutongo area

The Kibara orogen is characterised by the presence of several granite generations. The main granite generation (the former G1-3 granites) intruded at 1380 ± 10 Ma in the Palaeo- and Mesoproterozoic rocks (Kokonyangi et al., 2004, 2006; Tack et al., 2006; 2008) and is not mineralised. Historically, the Sn-mineralisation has been related to the so-called G4-granites, which are spatially associated and have been described as non-deformed equigranular muscovite granites (Cahen et al., 1967). These Kibara G4-granites have recently been dated with U-Pb SHRIMP zircon at 986 ± 10 Ma (Tack et al. 2006, 2008).

The major and trace element composition of the granites in the Kibara orogen has been investigated in numerous studies (e.g. Fernandez-Alonso et al., 1986; Lehmann & Lavreau, 1987). These studies were mainly carried out to distinguish differences in geochemical composition between possible granite generations (Fernandez-Alonso et al., 1986). However, no major systematic variations were observed, except for the G4-granites. The Kigali granite has been interpreted to belong to the youngest granite generation of the Kibara orogen (G4-granite). If we use the classification of Cerny et al. (2005), these G4-granites should be considered as

"parental granite for hydrothermal mineralisation" or "parental granite for a rare element pegmatite" (Dewaele et al., accepted). Although the major and minor element composition of this granite generation shows depletion and enrichment trends (Dewaele et al., accepted) typical for granites associated with rare element mineralisation (Cerny et al. 2005; Plimer 1987; Stemprok 1979), the average tin content of these G4-granites is below the minimum concentration for a typical tin mineralised granite (i.e. < 15 ppm, Cerny et al. 2005; Plimer 1987; Stemprok 1979). It is suggested that tin either was not enriched (opposed to all other typical rare elements) or that it has been mobilised during later hydrothermal events post-dating the crystallisation of the G4 granites. Redissolution and redistribution of tin during later hydrothermal events has been described from granite related tin deposits worldwide (eg. Groves & Taylor, 1973; Lehmann & Harmanto, 1990; Halter et al. 1998, Kontak & Clark, 2002).

7.2 Structural setting of the Sn-mineralised quartz veins

Peeters (1956), Aderca (1957), Lhoest (1957a, b) and Pohl (1974, 1975) investigated the structural setting of the Sn-mineralised veins in the Rutongo area and proposed a relative time relationship between deformation (folding at different scales, faulting and thrusting), granite intrusion and mineralisation. These authors describe that large scale folding of the area occurred due to EW compression, forming the large west-verging Rutongo anticline. Axial planar cleavage developed in the metapelitic rocks and refracted cleavage or fractures formed in the quartzites. Folding progressively continued and folds were breached through along NS-trending, east-dipping low-angle thrust faults in the core of the anticline. During a late to post-tectonic phase, a granite batholith (i.e. Kigali granite) intruded the south-eastern part of the anticline, which resulted in doming of the overlying layers (Lhoest, 1957a, b; Pohl, 1975). Finally, the fractures were opened and filled by hydrothermal fluids from the granite. However, the authors do not agree on the relative timing of the NS-trending thrust faults and the formation of the mineralised veins. Lhoest (1957a) states the faults formed before the emplacement of the granites, Pohl (1975) places their formation after granite intrusion but contemporaneous with vein formation, whereas Peeters (1956) states their emplacement is post-vein formation. Pohl (1975) remarks the NS-trending thrusts could not be younger than the Sn-mineralised veins because the veins did not experience considerable deformed or rotation since their formation.

The authors also disagree on the processes which caused formation of the Sn-mineralised veins. According to Aderca (1957), the mineralised quartz veins of Rutongo are the result of "large scale boudinage". Longitudinal stretching of the layers was the result of an intense compression, which was oriented nearly perpendicular to the orientation of the beds. The quartzite beds adapted to this compression by layer-parallel extension, which resulted in segmentation (Aderca, 1957). However, Aderca (1957) does not specify when this process happened with regard to the general evolution of the area. He refers by geometric analogy to the "boudins" developed in the Bastogne area (High-Ardenne Slate belt, Belgium), where they were described for the first time (Lohest et al., 1908). At the time, the genetic significance of the term boudinage had already the nowadays widely accepted definition (e.g. Cloos, 1947) of the process of layer-parallel extension of competent layers, which are embedded in an incompetent matrix, with possibly the development of interboudin veins (Sintubin et al., 2000; Kenis et al., 2002; van der Pluijm & Marshak, 2004). However, based on the geometry of the cracks in the Rutongo area, it appears unrealistic that the Sn-mineralised veins formed by this kind of layer-parallel extension. In the third dimension, the veins are not perpendicular to a single layer, but rather crosscut several layers and do not look like typical "sausage-like" structures, as would be the case if boudinage was the responsible formation process.

According to Lhoest (1957a), the general NS orientation of the Sn-mineralised quartz veins is subparallel to the overall direction of the structural grain. Therefore, he interprets the fractures, which host the Sn-mineralised veins, to be contemporaneous with major EW folding. The intrusion of the granite caused subsequently the formation of small EW-trending secondary folds and thrust faults in the anticline. The author suggests also that the previously formed fractures in the quartzite layers were opened due to this granitic doming and were subsequently filled with cassiterite-bearing quartz. The alteration at the base of the quartzite layers might indicate that this contact zone served as a pathway for the mineralising fluids (Lhoest, 1957b). Lhoest (1957a) remarks that the quartzite units west of the thrust fault in the core of the anticline, although fractured, do not contain Sn-mineralised veins, notwithstanding the fact that they are located at the same stratigraphic level as those located east of the fault and which are mineralised. In his model, the NS-trending thrust faults predate mineralisation and acted as a barrier for the mineralising fluids. The pre-existence of fracture planes is refuted by Pohl (1975), who states that fracture development in the competent beds would also have resulted in a general cleavage development in the metapelitic rocks, which is not the case. He also rejects the possibility of fracture opening by magmatic doming since no Sn-mineralised veins were observed at the Nyirabukingule dome and radially dispersed Sn-mineralised veins, which would be expected, were not observed at the Nyabugogo dome.

Pohl (1974, 1975) interpreted that the Sn-mineralised quartz veins formed late in the main deformation, i.e. when the core of the anticline was closed and deformation was only possible by thrust faulting. This resulted in an important deformation of the eastern flank of the anticline. The fractures formed because the front part of the overthrust block moved faster than its roots towards the

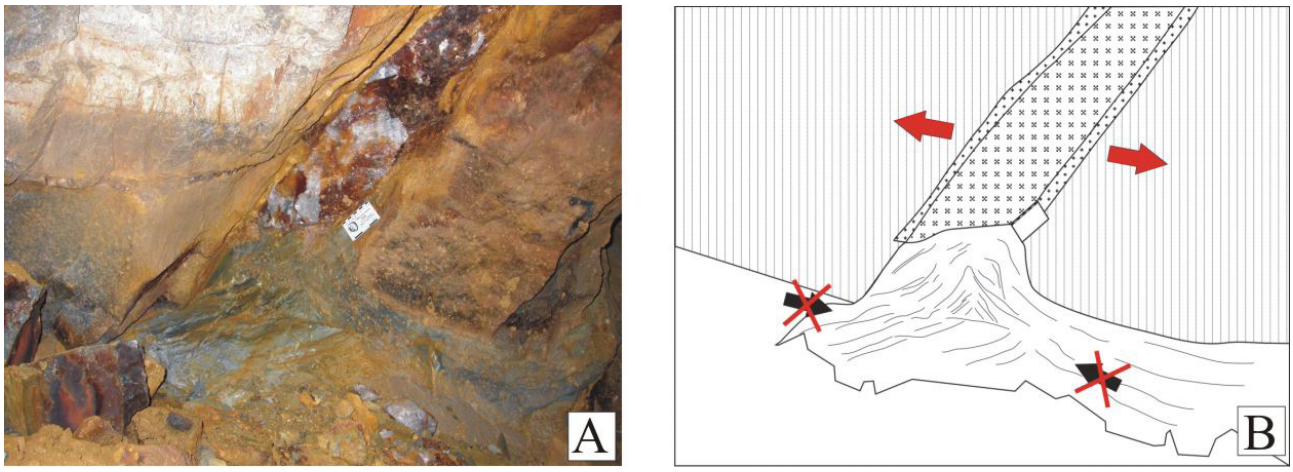

Figure 7. Picture (A) and drawing (B) of a Sn-mineralised quartz vein at Masoro. The vein is hosted by a quartzite bed and stopped at the bottom by shale. At the margins of the vein a centimetre thick muscovite alteration zone is present. σ_3 is indicated by red arrows. Scale bar is 9 cm.

west (Pohl, 1975). During their formation, the fractures were filled by a hydrothermal fluid originating from the granite (Pohl, 1975). According to Pohl (1975), the small secondary EW-trending folds formed contemporaneous with the main fold, before intrusion of the granite and thrust faulting. Our own field observations are difficult to reconcile with the compressional setting proposed by Pohl (1975). Fig. 7 shows the trajectory of the foliation planes in metapelitic layers in the vicinity of a Sn-mineralised quartz vein, which is hosted by a competent quartzite bed. The fold-like structure in the metapelitic rocks could be interpreted as the result of foliation parallel shortening. However, this is in contradiction with the presence of the vein-fracture, which formed in an extensional setting. Therefore, the structure is interpreted as a passive entering of the foliation planes into the cavity created during the opening of the fracture. Both opening of the fracture and the plastically deformed foliation planes suggest a maximum compressive stress oriented at high angle to the bedding. Since bedding has an orientation of ~15°, a vertical maximum compressive stress in an extensional regime is more likely than a horizontal compressive stress. During extension, the direction of minimal stress (σ_3) was oriented ~EW.

As advocated by the different authors, there is no evidence that the Sn-mineralised quartz veins (or precursor fracture planes) formed before the main folding event. This would cause a fan-shaped dip direction across the anticline. In the eastern flank of the anticline, there is almost no variation in the dip of these veins (Lhoest, 1957a; Pohl, 1975). In the western flank of the anticline, only unmineralised bedding parallel quartz veins have been observed, which dip to the west (Lhoest, 1957a). The large anticline formed due to EW compression, during which it is unlikely to form NS-trending veins, except when bedding is at high angle to σ_1. In addition, Sn-mineralisation is related to the intrusion of the G4-granite, which post-dates general folding. The relative timing of the veins with respect to the formation of the secondary EW-trending folds is still a matter of discussion. During formation of the NS-trending Sn-mineralised veins, the direction of maximum principal stress (σ_1) could have been oriented horizontally or vertically. In the first case ($\sigma_h > \sigma_v$), σ_1 was oriented NS. In this case, the development of the veins could have occurred prior, contemporaneous with or after the formation of the EW-trending secondary folds, in a late phase of deformation. Since the orientation of the veins is almost perpendicular to the axis of the secondary folds, the veins could have been rotated during folding without any change in dip orientation. In the second case ($\sigma_h < \sigma_v$), σ_1 was oriented vertically and the veins developed during uplift, after deformation of the area. The second option could be preferred if the relationship between the mineralised fractures and the plastically deformed foliation planes are considered, which favours a vertical maximum compressive stress in an extensional regime. Anyhow, the structural setting of the mineralised veins indicates a relatively late formation in the general evolution of the Rutongo anticline.

7.3 Fluid flow in the Rutongo area

An exploratory microthermometric investigation has been carried out by Günther (1990). He measured inclusions in different quartz and cassiterite samples, of which, however, the paragenetic position was not determined. Based on the presence of additional gas components and the volume of the gas bubble, he made a classification of four types of inclusions (Fig. 8); group SIA/C and SIID/E are inclusions with a H_2O-CO_2-N_2-CH_4-NaCl composition. The difference between both groups SIA/C and SID/E is that the gas bubble of group SIA/C inclusions homogenises to the liquid phase, and the gas bubble of most group SID/E inclusions homogenises to the gas phase. Group SII are aqueous inclusions that often contain a daughter mineral, while group SIII are aqueous inclusions without a daughter mineral.

Notwithstanding this work, the exact relationship between the different fluid types and the cassiterite mineralisation itself was not indicated. To determine which fluid was responsible for the cassiterite mineralisation, preliminary microthermometric measurements were carried out on samples from the Nyamiumba mineralisation (Dewaele et al., 2007b). No primary inclusions oriented along growth zones can be found within the quartz and cassiterite crystals. Most fluid inclusions in quartz crystals are randomly distributed, but there are some inclusions that occur along secondary trails that are directed towards cassiterite mineralisation. Therefore, these are interpreted to be representative for the fluids responsible for mineralisation (cf Dewaele et al., 2004; El Desoucky et al., 2008). Fluid inclusions in cassiterite crystals are randomly distributed or occur along cleavage planes. Cassiterite shows indication for intense fracturing and recrystallisation along crystallographic planes. Where fracture planes are developed, randomly distributed fluid inclusions are decrepitated, which indicates that these belong to an earlier generation.

Although no primary fluid inclusions have been found, the fluids in the trails towards mineralisation in the quartz crystals and the randomly distributed inclusions in the cassiterite crystals are considered representative for fluids related to cassiterite mineralisation (Dewaele et al., 2007b). Cassiterite precipitation is interpreted to have occurred from a H_2O-CO_2-(X)-NaCl (with X = CH_4-N_2; Günter 1990) fluid at a homogenisation (minimum formation) temperature between 220° and 300°C and Tm_{Ice} values between -12.7 and -4.4°C. These data correspond well to the SI fluid type identified by Günther (1990) (Fig. 8).

The mineralised quartz veins in the Rutongo area are associated with intense alteration of the host-rocks, represented by silicification, tourmalinisation, sericitisation and muscovitisation. The cassiterite mineralisation itself is associated with muscovite crystals in fractures in quartz veins. A similar paragenetic sequence can be observed for the cassiterite mineralisation in the pegmatites of the Gatumba area (Dewaele et al., 2007b, 2008). Cassiterite precipitation in these pegmatites is associated with an intense K-alteration (sericitisation and muscovitisation) that resulted from fluids with a H_2O-CO_2-(X)-NaCl-KCl composition (Th_{Tot} between 240° and 366°C; Tm_{Ice} between -19.2 and -8.2°C). Dewaele et al. (2007b, 2008) identified that K-alteration and cassiterite mineralisation clearly postdates columbite-tantalite mineralisation in the pegmatites.

7.4 Stable and radiogenic isotopes

Many existing combined stable isotope and fluid inclusion studies trace the origin of tin-mineralising fluids (references in Heinrich, 1990; Taylor, 1997, Jackson et al., 2000). Some indicate a direct input of magmatic fluids (Sun & Eadington, 1987), whilst the majority shows a mixture of dominantly magmatic fluids with meteoric fluids that equilibrated with granite at 600°C to 400°C. Heinrich (1990) suggested that irrespective of the ambiguity regarding the ultimate source of H_2O, the stable isotope data from nearly all deposits indicate that tin-mineralising fluids were equilibrated isotopically with a hot (>400°C) granite source rock, prior to transport into a cooler depositional environment. Transport of hot fluids into a cooler environment involves structural focussing and prevention of complete chemical equilibrium with wall-rocks.

The calculated stable isotope composition of the ambient fluids of the cassiterite plots adjacent to the field of primary magmatic fluids, whilst that of the ambient fluids of quartz falls into the field of metamorphic fluids (Fig. 5). It should be noted that fluid inclusions, which are interpreted to be directly related to cassiterite precipitation, dominate the population in cassiterite (Dewaele et al.

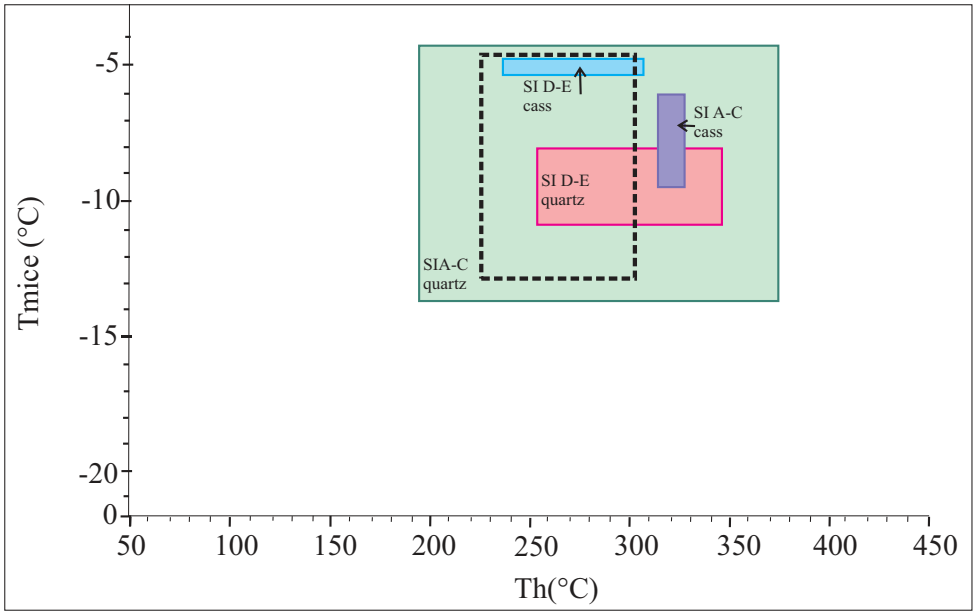

Figure 8. Tm_{Ice}-Th_{Tot} diagram showing the distribution of the different fluid types identified by Günther (1990), compared with the data of the ambient fluids related to the cassiterite mineralisation (dashed square; Dewaele et al., 2007b). Group SIA/C (green coloured square for fluid inclusions in quartz and purple coloured square for fluid inclusions in cassiterite) and SID/E (pink coloured square for fluid inclusions in quartz and light-blue coloured square for fluid inclusions in cassiterite) are inclusions with a H_2O- CO_2-N_2-(CH_4)-X-NaCl-X composition.

2007b), whereas secondary inclusions, arguably not related to the cassiterite mineralisation, are more dominant in the quartz crystals. The stable isotope composition of the fluids in the quartz veins would favour a metamorphic origin. The discrepancy of H isotopes can be explained in two ways. Either the δD signature of the fluids in Rutongo cassiterite directly indicates a magmatic origin. In this case, the signature would have been preserved due to a limited interaction between the fluids and the host-rock, reflected by the narrow alteration halos around the mineralised quartz veins. The shift in isotopic composition of the ambient fluids in cassiterite and quartz would then indicate a transition from circulation of magmatic fluids to a dominantly metamorphic system (cf Wilkinson, 1990; Wilkinson et al. 1995). Another explanation would be that the $\delta^{18}O$-δD signature reflects the interaction and equilibrium of metamorphic fluids with magmatic rocks (in this case granite in the basement) for the fluids precipitating the cassiterite. The stable isotope composition of the fluids in the quartz veins would then indicate metamorphic fluids that did not equilibrated with the granitic rocks. Given the probable co-precipitation of the two phases (same calculated formation temperature), their established O isotope equilibrium and the suggested remobilisation of Sn in the granitic rocks, the second explanation is favoured.

This intense interaction between circulating fluids and the host-rock during late stages in the formation of the Rutongo vein system is indicated by the Pb isotopic composition of sulphides present in the cassiterite mineralised quartz veins. These sulphides (galena, pyrite and arsenopyrite) formed after the cassiterite. The similarity of the Pb isotope ratios of the sulphides in the quartz veins and the diagenetic pyrite in the surrounding host-rock favours that Pb originated from pyrite in the surrounding sedimentary rocks (cf Pohl, 1994) and that the Pb was homogenised prior to precipitation of the sulphides in the quartz veins.

7.5 Timing of the cassiterite mineralisation in the Rutongo area

After intrusion of the G4-granites (986 ± 10 Ma, Tack et al., 2006; 2008), pegmatites were emplaced at 968 ± 8 Ma (Brinckman & Lehmann, 1983). The pegmatites are mineralised with columbite-tantalite and cassiterite. Recent investigation by Dewaele et al. (2007a, 2008) indicates that the columbite-tantalite mineralisation is contemporaneous with the crystallisation of the pegmatites, whereas the cassiterite present in the pegmatites formed during a later phase of intense K-alteration (sericitisation and muscovitisation). In addition, it has been reported that pegmatites are sometimes crosscut by a generation of cassiterite-mineralised quartz veins (Varlamoff, 1956; 1969). It should, on the other hand, be noted that Varlamoff (1956) and many geologists of former Belgian colonial mining companies (unpublished mining archives of the MRAC) described different generations of quartz veins, of which some of them are crosscut by pegmatites. The exact paragenetic position of the cassiterite mineralised generation of quartz veins is, however, mostly not indicated. The emplacement of the cassiterite mineralised quartz veins has been dated at 951 ± 18 Ma in Burundi (Rb-Sr muscovite; Brinckman et al., 1994).

The new apparent age obtained in our investigation (869 ± 7 Ma) is much younger than the accepted ages for the G4-granite, younger than the Kibara pegmatites and associated columbite-tantalite mineralisation and younger than the age reported for the Sn-mineralised quartz vein (Brinckman et al., 2001). Looking at other published data, the newly obtained age is, however, not exceptional. Monteyne-Poulaert et al. (1962a, b) obtained Rb-Sr ages of muscovites from different Nb-Ta-Sn-mineralised pegmatites and Sn-mineralised quartz veins from D.R.Congo (Kivu), Rwanda and Burundi that range between ca 1100 and 870 Ma. The authors interpreted this range of ages to be caused by different post-tectonic thermal events. Cahen & Snelling (1966) place the formation of post-tectonic pegmatites and veins with cassiterite and sulphides between 1000 ± 30 Ma and 870 ± 26 Ma for the Rwandese-Burundese part of the Kibara orogen, based on a compilation of published K/Ar, Rb/Sr, U/Pb and Pb-Pb ages. Brinckmann (1988) dated muscovite crystals from Sn-mineralised quartz veins and from altered host-rocks at Mulehe, Burundi, which yielded a Rb-Sr age of 936 ± 82 Ma. The K-Ar age determinations, however, yielded apparent ages between 840 and 780 Ma, with an age cluster between 830-800. The author interpreted the K-Ar ages as indication for late thermal or thermodynamic events during which the K-Ar ratio was altered. In addition, Ikingura et al. (1992) carried out ^{40}Ar-^{39}Ar dating on micas from granites in the Karangwe-Ankolean (Kibara orogen in the northwestern part of Tanzania) and obtained ages in a range between 945-700 Ma. This range has been interpreted as indicative of partial gas loss as a result of thermal overprinting.

The integrated age of 869 ± 7 Ma obtained in this study could have several implications. First, it could directly identify that the cassiterite mineralisation postdates the G4-granite emplacement and the pegmatite formation. Secondly, it could just indicate the time period when the hydrothermal system dropped below the closing temperature of muscovite (~350°C) after a long period of cooling. The formation temperature of the cassiterite is calculated at ~ 400°C, based on the isotopic equilibrium between cassiterite and quartz and based on the pressure-corrected homogenisation temperature of fluid inclusions (Günther, 1990). The discrepancy between the formation temperature and closing temperature of muscovite could imply that the age of 869 ± 7 Ma would not directly reflect the age of the cassiterite precipitation. However, multiple recent studies indicate that the cooling period of tens and certainly more than 100Ma is unrealistic for a hydrothermal system directly linked to the cooling of a granite. In recent discussions, a cooling period of 20Ma is even questioned. Different magmatic pulses are proposed for such a time elapse. It can, therefore, be postulated that the age of 869

± 7 Ma obtained in this study does not necessarily contribute to our understanding of the age of cassiterite mineralisation with regard to the age of the G4-granite emplacement and pegmatite formation. Thirdly, the age could indicate the time when the muscovite crystals have been recrystallized due to a younger hydrothermal event, not related to the G4-granite emplacement. Granites associated with rare element mineralisation often have high contents of heat-producing elements, due to which they can act as regional thermal anomalies for long periods after the emplacement of the granites, i.e. 10 to 30 Ma after initial emplacement of the granites (cf Jackson et al. 1989, Willis-Richards & Jackson, 1989; Kontak & Clark, 2002; Zhao et al., 2004), with temperatures above the closing temperature of muscovite (~ 350°C). However, Alderton & Harmon (and references herein) report hydrothermal activity associated with Sn-, W-, Cu-, Pb-, Zn mineralisation up to 100 Ma after granite consolidation. But in this case, the Sn-mineralisation is mainly formed during the early phases. In the past, authors have interpreted ages in the Kibara fold belt – younger than the granite emplacement period at ~1400Ma and ~1000Ma – to be related to different post-Kibaran tectonothermal events (Monteyne-Poulaert et al., 1962a, b; Cahen & Snelling, 1966; Brinckmann, 1988; Ikingura et al., 1992). Several events affecting the Kibara belt, postdating the intrusion of the G4-granite generation, which could have caused thermal overprinting, have been described in literature. According to Monteyne-Poulaert et al. (1962b), after the emplacement of the pegmatites a late phase of U-mineralisation took place around 845 Ma (U-Pb on uraninite and cyrtolite). Another possible heat source for thermal overprinting could be Neoproterozoic magmatic intrusions. In central and southern Africa there is evidence of widespread within-plate and rift-related magmatism at ~1000-710 Ma (Hanson, 2003). These alkaline plutonic centres in the Kibara belt reflect uprise of mantle-derived magmas along older lines of structural weakness in the same time frame (Hanson, 2003). Kampunzu et al. (1998) determined Rb-Sr whole rock ages of three Neoproterozoic igneous complexes in Kivu (D.R.C.), which are composed of undersaturated silicate rocks.

Based on the arguments above, it is suggested that the integrated age probably indicates a resetting of the muscovites, which occur associated with the cassiterite mineralisation, during a hydrothermal event post-dating the emplacement and cooling of the Kigali granite and not directly related to the cassiterite precipitation. It infers that the integrated Ar-Ar age would only indicate a minimum age for the cassiterite mineralisation, while the pegmatite emplacement and associated columbite-tantalite mineralisation age would indicate a maximum age (~965 ± 5 Ma; Romer & Lehmann 1995). Hydrothermal circulation – and interaction with the host-rocks – clearly existed after the formation on the cassiterite, as is illustrated by the Pb-isotopes of the sulphides that formed after the cassiterite in the quartz veins.

7.6 Conclusions

For the Kibara orogen, it is postulated that the main granite generation G1-3 intruded at 1380 ± 10 Ma in the Palaeo- and Mesoproterozoic rocks. These granites are not associated with mineralisation. At 986 ± 10 Ma, the G4-granites, such as the Kigali granite, were emplaced. It can be observed that these G4-granites show depletion and enrichment trends typical for granites associated with rare element mineralisation (Dewaele et al. in publication). The average tin content of these granites is below the minimum concentration of typical tin-mineralised granites. Since Sn is not enriched in such a way as the other typical elements for rare element granites, it is suggested that Sn has been mobilised during hydrothermal events post-dating the crystallisation of the G4-granites. After emplacement of these G4-granites, pegmatites were intruded at 968 ± 8 Ma. Some of these pegmatites are associated with columbite-tantalite mineralisation. The columbite-tantalite has been dated in Burundi at 962 ± 2 Ma, which overlaps with the timing of pegmatite emplacement. In the Gatumba area, the cassiterite mineralisation and the associated K-alteration clearly postdate the columbite-tantalite mineralisation, as observed by their crosscutting relationship. Fluids and metals were introduced along fractures and faults.

Structural analysis indicates that the mineralised veins formed due to extension, with maximum compressive stress at high angle to the bedding. Combined with the formation of the secondary E-W oriented folds, it would seem that the maximal compressive stress would have been oriented vertical. This would imply that veins formed during uplift, i.e. clearly after the formation of the N-S oriented fold and granite emplacement. The obtained age can probably not directly be related to the formation of the cassiterite mineralisation, but is interpreted to reflect a younger hydrothermal event.

Although there is no single straightforward argument to directly exclude a magmatic-hydrothermal origin of the cassiterite mineralisation, it is postulated, based on the structural setting, petrographical observations, geochemistry of the G4-granites and stable isotope geochemistry, that the Sn was transported syn- to post-deformation by metamorphic fluids, clearly after formation of the Rutongo anticline, G4-granite crystallisation (and pegmatite emplacement). The metamorphic fluids that precipitated the cassiterite are in stable isotopic equilibrium with the magmatic rocks and could have remobilised the Sn from these granites, which have now a Sn concentration below the limit for a typical tin-mineralised granite. The circulation of the fluids resulted in precipitation of cassiterite in structural traps at temperatures around ~400°C and promoted intense alteration of the host-rock of the quartz veins. A maximum age for the cassiterite crystallisation would be the age of pegmatite emplacement (965 ± 5 Ma), while the newly obtained apparent Ar-Ar age (869 ± 7 Ma), which is interpreted to reflect a hydrothermal resetting, would reflect a minimum age.

8. Acknowledgements

The work of Friso De Clercq is supported by the Institute for the promotion of Innovation through Science and Technology in Flanders (IWT-Vlaanderen). Herman Nijs and Rene Boyen kindly prepared the numerous thin and polished sections and the doubly-polished wafers. Colleagues of the former REDEMI in Rwanda (Dr Michael Biryabarema, Ir Jean Ruzindana and Jean-Bosco Rusanganwa) are thanked for access to the different mine sites in the Rutongo area during our first period of fieldwork. Mr Leonidas Simpenzwe and Mr Martin Kahanovitz of Eurotrade International S.A.R.L. are thanked for the access and logistic help at Rutongo during recent fieldwork. The authors are especially thankful to H. Van Balen for helpful and constructive discussions. The text has largely improved by the comments of two reviewers, Mr Michel Gauthier and an anonymous reviewer.

9. References

ADERCA, B., 1957. Un cas de « Boudinage » à grande échelle: la mine de Rutongo au Rwanda. *Annales de la Société Géologique de Belgique*, 80: 279-285.

AGASSIZ, J.F., 1954. Géologie et pegmatites stannifères de la région Mumba-Numbi, Kivu (Congo belge). *Comité National du Kivu, nouvelle série*, 7.

ALDERTON, D.H.M & HARMON, R.S., 1991. Fluid inclusion and stable isotope evidence for the origin of mineralising fluids in south-west England. *Mineralogical Magazine*, 55: 605-611.

BAUDET, D., HANON, M., LEMONNE, E. & THEUNISSEN, K., 1988. Lithostratigraphie du domaine sédimentaire de la chaîne Kibarienne au Rwanda. *Annales de la Société Géologique de Belgique*, 112: 225-246.

BERTOSSA, A., GÉRARDS, J. & PETRICEC, V., 1964. Géologie de la région de Kigali. *Bulletin du Service Géologique de Rwanda*, 1: 3-12.

BRINCKMANN, J., 1988. The post-Kibaran tin and tungsten mineralization in north Burundi (Mulehe and Nyabisaka). *International Geological Correlation Programme, Project n° 255, TU Braunschweig-MRAC Tervuren*, 1: 7-9.

BRINCKMANN, J. & LEHMANN, B., 1983. *Exploration de la bastnaésite-moncite dans la région de Gakara, Burundi. Rapport sur la phase 1*. Unpublished report, Bujumbura/Hannover, 157 pp.

BRINCKMANN, J., LEHMANN, B. & TIMM, F. 1994. Proterozoic gold mineralisation in NW Burundi. *Ore geology reviews*, 9: 85-103.

BRINCKMANN, J., LEHMANN, B., HEIN, U., HOHNDORF, A., MUSSALLAM, K., WEISER, Th. & TIMM, F., 2001. La géologie et la minéralisation primaire de l'or de la chaîne Kibarienne, Nord-Ouest du Burundi, Afrique orientale. *Geologisches Jahrbuch Reihe D,* 101: 195 pp.

BURGESS, R., KIVIETS, G.B. & HARRIS, J.W. 2004. $^{40}Ar/^{39}Ar$ age determinations of eclogitic clinopyroxene and garnet inclusions in diamonds from the Venetia and Orapa kimberlites. Lithos, 77: 113–124.

CAHEN, L. & SNELLING, N.J., 1966. *The geochronology of Equatorial Africa*. North-Holland Publishing Company, Amsterdam.

CAHEN, L., DELHAL, J. & DEUTSCH, S., 1967. Rubidium-strontium geochronology of some granitic rocks from the Kibaran belt (Central Katanga, Rep. of the Congo). *Annales des Sciences Géologiques Musée Royal de l'Afrique Centrale, Tervuren, Belgium. Série in 8°*, 59, 65 pp.

CAHEN, L., SNELLING, N.J., DELHAL, J., VAIL, J.R., BONHOMME, M. & LEDENT, D., 1984. *The geochronology and evolution of Africa*, Clarendon Press Oxford, 512 pp.

CAUET, S. & POHL, W., 1988. *Lead isotope composition of sulphide minerals from Kibaran mineralisations in Rwanda*. Metallogeny of the Kibara belt, Central Africa. International Geological Correlation Program 255. Newsletter 1: 11-14.

CERNY, P., BLEVIN, P.L., CUNEY, M. & LONDON, D., 2005. Granite-related ore deposits. *In* Hedenquist, J.W., Thompson, J.F.H., Goldfarb, R.J., Richards, J.P.(eds), *Economic Geology: One hundredth Anniversary Volume: 1905-2005,* 337-370.

CLOOS, E., 1947. Boudinage. *Transactions of the American Geophysical Union*, 28: 628-632.

DE CLERCQ, F, MUCHEZ, Ph., DEWAELE, S. & BOYCE, A. 2008. The tungsten mineralisation at Nyakabingo and Gifurwe (Rwanda): preliminary results. *Geologica Belgica,* 11: 251-258.

DE KUN, N., 1954. Les pegmatites du Nord Lugulu. *Annales de la Société Géologique de Belgique,* 78: 27-30.

DE KUN, N., 1959. Les gisements de cassitérite de de columbo-tantalite du Nord Lugulu, Kivu, Congo belge. *Annales de la Société Géologique de Belgique*, 82: 81-196.

DEWAELE, S., MUCHEZ, Ph. & BANKS, D.A., 2004. Fluid evolution along multistage composite fault systems at the southern margin of the Lower Palaeozoic Anglo-Brabant fold belt, Belgium. *Geofluids*, 4: 341-356.

DEWAELE, S., TACK, L. & FERNANDEZ, M., accepted. Cassiterite and columbite-tantalite (coltan) mineralisation in the Mesoproterozoic rocks of the northern part of the Kibara orogen (Central Africa): preliminary results. *Mededelingen der zittingen van de Koninklijke Academie voor Overzeese wetenschappen*.

DEWAELE, S., TACK, L., FERNANDEZ, M., BOYCE, A. & MUCHEZ, Ph., 2007a. Cassiterite and columbite-tantalite mineralisation in pegmatites of the northern part of the Kibara orogen (Central Africa): the Rutongo area (Rwanda). *In* Andrew, C.J. et al. (eds) *Proceedings of the 9th Biennal SGA meeting. Mineral exploration and research: digging deeper 20th–23rd August 2007. Dublin, Ireland, 1489-1492*.

DEWAELE, S., TACK, L., FERNANDEZ, M., BOYCE, A. & MUCHEZ, Ph., 2007b. Cassiterite mineralisation in vein-type deposits of the Kibara orogen (Central Africa): Nyamiumba (Rutongo area, Rwanda). *In* Andrew, C.J. et al. (Eds) *Proceedings of the 9th Biennal SGA meeting. Mineral exploration and research: digging deeper 20th–23rd August 2007. Dublin, Ireland, 1007-1010.*

DEWAELE, S., TACK, L., FERNANDEZ-ALONSO, M., BOYCE, A., MUCHEZ, Ph., SCHNEIDER, J., COOPER, G. & WHEELER, K., 2008. Geology and mineralisation of the Gatumba area, Rwanda: Present state of knowledge. *Etudes Rwandaises,* 16: 6-24.

EL DESOUKY, H., MUCHEZ, Ph., DEWAELE, S., BOUTWOOD, A. & TYLER, R. 2008. Postorogenic Origin of the Stratiform Cu Mineralisation at Lufukwe, Lufilian Foreland, Democratic Republic of Congo. *Economic Geology,* 103: 555-582.

FALLICK, A.E., JOCELY, J. & HAMILTON, P.J., 1987. Oxygen and hydrogen stable isotope systematics in Brazilian agates. *In* Rodriquez, C. (ed.), *Geochemistry of the Earth Surface and Processes of Mineral Formation*. Instituto de Geologica (CSIC), Madrid, 99– 117.

FERNANDEZ-ALONSO, M., LAVREAU, J. & KLERKX, J., 1986. Geochemistry and geochronology of the Kibaran granites in Burundi, Central Africa: implications for the Kibaran orogeny. *Chemical Geology*, 57: 217-234.

FERNANDEZ-ALONSO, M. & THEUNISSEN, K., 1998. Airborne geophysics and geochemistry providing insights in the intracontinental evolution of the Mesoproterozoic Kibaran belt (Central Africa). *Geological Magazine*, 135: 203-216.

FORSTER, M.A. & LISTER, G.S. 2004. The interpretation of Ar-40/Ar-39 apparent age spectra produced by mixing: application of the method of asymptotes and limits. *Journal of Structural Geology*, 26, 2: 287-305.

GERARDS, J. & LEDENT, D., L. 1970. Grands traits de la géologie du Rwanda, différents types de roches granitiques et premières données sur les ages de ces roches. *Annales de la Sociéte Géologique de Belgique*, 93: 477-489.

GROVES, D.I. & TAYLOR, R.G., 1973. Greisenisation and mineralisation at Anchor tin mine, northeast Tasmania. *Transactions of the Institute of Mining and Metallurgy*, 135-146.

GUNTHER, M.A., 1990. *Flüssigkeitseinschlüsse und geologisches Umfeld zentralafrikanischer Sn-, W- und Au-Lagerstätten (Rwanda and Burundi)*. Unpublished PhD thesis Naturwissenschaftlichen Fakultät der technischen Universität Carolo-Wilhelmina zu Braunschweig, 144 pp.

HALTER, W.E., WILLIAM-JONES, A.E. & KONTAK, D.J., 1998. Modelling fluid-rock interaction during greisenisation at the East Kemptville tin deposit: implications for mineralisation. *Chemical Geology*, 150: 1-17.

HANSON, R.E., 2003. Proterozoic geochronology and tectonic evolution of southern Africa. *In* Yoshida, M., Windley, B.F. & Dasgupta, S. (eds), *Proterozoic East Gondwana: Supercontinent Assembly and Breakup*. Geological Society, London, Special Publications, 206: 427-463.

HEINRICH, C.A., 1990. The chemistry of hydrothermal tin(-tungsten) ore deposition. *Economic Geology,* 85: 457-481.

IKINGURA, J.R., REYNOLDS, P.H., WATKINSON, D.H. & BELL, K., 1992. $^{40}Ar/^{39}Ar$ dating of micas from granites of NE Kibaran belt (Karangwe-Ankolean), NW Tanzania. *Journal of African Earth Sciences*, 15: 501-511.

JACKSON, N.J., WILLIS-RICHARDS, J., MANNING, D.A.C. & SAMS, M.S., 1989. Evolution of the Cornubian Ore Field, Southwest England: Part II. Mineral deposits and ore-forming processes. *Economic Geology*, 84: 1101-1133.

JACKSON, P., CHANGKAKOTI, A., KROUSE, H.R. & GRAY, J., 2000. The origin of greisen fluids of the Foley's zone, Cleveland tin deposit, Tasmania, Australia. *Economic Geology*, 95: 227-236.

JOURDAN, F., VERATI, C. & FERAUD, G., 2006. Intercalibration of the Hb3gr $^{40}Ar/^{39}Ar$ dating standard. *Chemical Geology*, 231: 77–189.

KAMPUNZU, A.B., RUMVEGERI, B.T., KAPENDA, D., LUBALA, R.T. & CARON, J.P.H., 1986. Les Kibarides d'Afrique centrale et orientale: une chaîne de collision. *UNESCO. Geology for Development Newsletter*, 5: 125-137.

KAMPUNZU, A.B., KRAMERS, J.D. & MAKUTU, M.N., 1998. Rb-Sr whole rock ages of the Lueshe, Kirumba and Numbi igneous complexes (Kivu, Democratic Republic of Congo) and the break-up of the Rodinia supercontinent. *Journal of African Earth Sciences, 26: 29-36.*

KENIS, I., SINTUBIN, M., MUCHEZ, Ph. & BURKE, E.A.J., 2002. The "boudinage" question in the High-Ardenne Slate Belt (Belgium): a combined structural and fluid-inclusion approach. *Tectonophysics*, 348: 93-110.

KLERKX, J., LIEGEOIS, J.P., LAVREAU, J. & THEUNISSEN, K., 1984. Granitoides kibariens précoces et tectonique tangentielle au Burundi : magmatisme bimodal lié à une distension crustale. *In* Klerkx, J. & Michot, J. (eds), *African Geology, A volume in honour of L. Cahen*. Musée Royale d'Afrique Centrale, Tervuren, 29-46.

KLERKX, J., LIEGEOIS, J.P., LAVREAU, J. & CLAESSENS, W., 1987. Crustal evolution of the northern Kibaran Belt, Eastern and Central Africa. *In* Kröner, A. (ed.), Proterozoic lithospheric evolution. *Geodynamics series (American Geophysics Union)*, 17: 217-233.

KOKONYANGI, J.W, ARMSTRONG, R., KAMPUNZU, A.B., YOSHIDA, M. & OKUDAIRA, T., 2004. U-Pb zircon geochronology and petrology of granitoids from Mitwaba (Katanga, Congo): implications for the evolution of the Mesoproterozoic Kibaran belt. *Precambrian Research*, 132: 79-106.

KOKONYANGI, J.W., KAMPUNZU, A.B, ARMSTRONG., R., YOSHIDA, M., OKUDAIRA, T., ARIMA, M. & NGULUBE, D.A., 2006. The Mesoproterozoic Kibaride belt (Katanga, D.R. Congo). *Journal of African Earth Sciences*, 46: 1-35.

KONTAK, D.J. & CLARK, A.H., 2002. Genesis of the giant, bonanza San Rafael Lode tin deposit, Peru: origin and significance of pervasive alteration. *Economic geology*, 97: 1741-1777.

LEGRAYE, M., 1955. Quelques observations sur les pegmatites de la région de Kabunga (Kivu, Congo belge). *Annales de la Société Géologique de Belgique*, 78: 31-40.

LEHMANN, B. & LAVREAU, J., 1987. Tin granites of the northern Kibaran belt, Central Africa (Kivu/Zaire, Rwanda, Burundi). *In* Matheis, G. & Schandelmeier, H. (eds), *Current research in African earth sciences*. Balkema, Rotterdam, 33-36.

LEHMANN, B. & HARMANTO, A., 1990. Large-scale tin depletion in the Tanjungpandan tin granite, Belitung Island, Indonesia. *Economic Geology*, 85: 99-111.

LHOEST, A., 1957a. Les différents types de filons de la concession Somuki à Rutongo. *Annales de la Société Géologique de Belgique*, 80: 503-530.

LHOEST, A., 1957b. Note préliminaire sur la géologie de la région Kigali-Rutongo dans le Ruanda. *Bulletin de la Société Belge de Géologie*, 66: 190-198.

LOHEST, M., STAINIER, X. & FOURMARIER, P., 1908. Compte rendu de la session extraordinaire de la Société Géologique de Belgique, tenue à Eupen et à Bastogne les 29, 30 et 31 août et le 1, 2 et 3 septembre 1908. *Annales de la Société Géologique de Belgique*, 35: 351-434.

LUDWIG, K., 2003. *Isoplot/Ex, version 3: A Geochronological Toolkit for Microsoft Excel*. Geochronology Center, Berkeley, USA.

MONTEYNE-POULAERT, G., DELWICHE, R. & CAHEN, L., 1962a. Age de minéralisations pegmatitiques et filoniennnes du Rwanda et du Burundi. *Annales de la Société Géologique de Belgique*, 71: 210-221.

MONTEYNE-POULAERT, G., DELWICHE, R., SAFIANNIKOFF, A. & CAHEN, L., 1962b. Ages de minéralisations pegmatitiques et filoniennes du Kivu méridional (Congo oriental). Indications préliminaires sur les âges de phases pegmatitiques successives. Annales de la Société Géologique de Belgique*, 71: 272-295*.

OHMOTO, H., 1986. Stable isotope geochemistry of ore deposits. *In* Valley, J.W., Taylor, H.P. & O'Neil, J.R. (eds), *Stable Isotopes in High Temperature Geological Processes*. Reviews in Mineralogy, 16: 419– 559.

PEETERS, L., 1956. Contribution à la géologie des terrains anciens du Ruanda-Urundi et du Kivu. *Annales du Musée Royale du Congo belge, Tervuren, série in 8°, Sciences Géologiques,* 16: 1-197.

PISUTHA-ARNOND, V. & OHMOTO, H., 1983. Thermal history and chemical and isotopic compositions of the ore-forming fluids responsible for the Kuroko massive sulphide deposits in the Hokuroku district of Japan. *In* Ohmoto, H., Skinner, B.J. (Eds.), *The Kuroko and Related Volcanogenic Massive Sulphide Deposits*. Economic Geology Monograph 5: 523– 558.

PLIMER, I.R., 1987. Fundamental parameters for the formation of granite-related tin deposits. *Geologische Rundschau*, 76: 23-40.

POHL, W., 1974. *Rapport préliminaire - Mission géologique Rutongo*. Unpublished report Somirwa, 15pp.

POHL, W., 1975. Die tektonische Kontrolle der Zinngänge von Rutongo, Rwanda (Afrika). *Mitteillungen der Osterreichischen Geologischen Gesellschaft*, 68: 89-107.

POHL, W., 1994. Metallogeny of the northeastern Kibara belt, Central Africa – Recent perspectives. *Ore Geology Reviews*, 9: 105-130.

POHL, W. & GUNTHER, M.A., 1991. The origin of Kibaran (late Mid-Proterozoic) tin, tungsten and gold quartz vein deposits in Central Africa: a fluid inclusion study. *Mineralium Deposita*, 26: 51-59.

ROMER, R.L. & LEHMANN, B., 1995. U-Pb columbite-tantalite age of Neoproterozoic Ta-Nb mineralisation in Burundi. *Economic Geology*, 90: 2303-2309.

RUMVEGERI, B.T., 1991. Tectonic significance of Kibaran structures in central and eastern Africa. *Journal of African Earth Sciences*, 13: 267-276.

SAFIANNIKOFF, A., 1955. Classification des pegmatites du Congo belge et du Ruanda-Urundi. *Annales de la Société Géologique de Belgique*, 78: 57-70.

SHEPPARD, S.M.F., 1986. Characterization and isotopic variations in natural waters. *In* Valley, J.W., Taylor, H.P. & O'Neil, J.R. (Eds.), *Stable Isotopes in High Temperature Geological Processes*. Reviews in Mineralogy, 16: 165–183.

SINTUBIN, M., KENIS, I., SCHROYEN, K., MUCHEZ, Ph., & BURKE, E.A.J., 2000. "Boudinage" in the High-Ardenne slate belt (Belgium), reconsidered from the perspective of the "interboudin" veins. *Journal of Geochemical Exploration*, 69: 511-516.

STEENSTRA, B., 1967. Les pegmatites du Maniema et du Rwanda et les roches de transition entre les aplites et les pegmaties du Maniema. *Mineralium Deposita*, 2: 271-285.

STEMPROK, M., 1979. Mineralised granites and their origin. *Episodes*, 3: 20-24.

SUN, S. & EADINGTON, P.J., 1987. Oxygen isotope evidence for the mixing of magmatic and meteoric waters during tin mineralisation in the Mole granite, New South Wales, Australia. *Economic Geology*, 82: 43 -52.

TACK, L., BAUDET, D., CHARTRY, G., DEBLOND, A., FERNANDEZ-ALONSO, M., LAVREAU, J., LIEGEOIS, J.-P., TAHON, A., THEUNISSEN, K, TREFOIS, Ph. & WINGATE, M., 2002a. The Northeastern Kibaran Belt (NKB) reconsidered: evidence for a c. 1370 Ma-old, repeatedly reactivated Kibara mobile belt, preceding the c. 1.0 Ga Rodinia Supercontinent assembly. *Abstract for the 19th Colloquium of African Geology, El Jadida, Morocco, 19-23 March 2002, Special Abstracts volume*.

TACK, L., FERNANDEZ-ALONSO, M., TAHON, A., WINGATE, M. & BARRITT, S., 2002b. The "Northeastern Kibaran Belt" (NKB) and its mineralisations reconsidered: New constraints from a revised lithostratigraphy, a GIS-compilation of existing geological maps and a review of recently published as well as unpublished igneous emplacement ages in Burundi. *Abstract for the 11th Quadrennial IAGOD Symposium and Geocongress, Windhoek (Namibia), 22-26 July 2002*.

TACK, L., FERNANDEZ-ALONSO, M., DE WAELE, B., TAHON, A., DEWAELE, S., BAUDET, D. & CUTTEN, H., 2006. The northeastern Kibaran belt (NKB): a long-lived intraplate history. *Extended Abstract of oral communication submitted to session 1 ("Geodynamics of Africa") of the 21st Colloquium of African Geology (CAG21) at Maputo (Mozambique), 3-5 July 2006,* 149-151.

TACK, L., WINGATE, M., DE WAELE, B., MEERT, J., GRIFFIN, B., BELOUSOVA, E.A., TAHON, A., FERNANDEZ-ALONSO, M., BAUDET, D., CUTTEN, H. & DEWAELE, S., 2008. The Proterozoic Kibaran Belt in Central Africa: intracratonic 1375 Ma emplacement of a LIP. *Abstract for the 22nd Colloquium African Geology (CAG22), 04-06.11.2008, Hammamet, Tunisia, Abstract volume, p. 89*.

TAYLOR, R.G., 1979. *Geology of tin deposits*. Developments in Economic Geology 11. Elsevier. New York. 543pp.

VAN DER PLUIJM, B.A. & MARSHAK, S. 2004. *Earth structure: an introduction to structural geology and tectonics, second edition*. W.W. Norton & Company, 656 pp.

VARLAMOFF, N., 1948. Gisements de cassitérite de la région de Kalima (Maniema, Congo belge). *Annales de la Société Géologique de Belgique*, 71: 194-237.

VARLAMOFF, N., 1950. Granites et minéralisation au Maniema (Congo belge). *Annales de la Société Géologique de Belgique*, 73: 111-163.

VARLAMOFF, N., 1954a. Répartition des types de pegmatites autour de la partie nord-ouest du grand massif granitique de Nyanza. *Annales de la Société Géologique de Belgique,* 78: 1-21.

VARLAMOFF, N., 1954b. Tendances actuelles dans l'étude des pegmatites à travers le monde; revue des travaux sur les pegmatites du Congo belge et du Ruanda-Urundi; proposition d'une classification des pegmatites du Congo belge et de Ruanda-Urundi. *Annales de la Société Géologique de Belgique*, 77: 245-267.

VARLAMOFF, N., 1954c. Transitions entre les aplites et les pegmatites dans les zones de contact des massifs granitiques des concessions de Symétain à Kalima (Maniema, Congo belge). *Annales de la Société Géologique de Belgique*, 77: 101-120.

VARLAMOFF, N., 1956. Transitions entre les pegmatites et les filons de quartz dans les massifs granitiques des régions stannifères du Maniema (Congo belge). *Annales de la Société Géologique de Belgique*, 79: 385-403.

VARLAMOFF, N., 1961. Pegmatites à amblygonite et à spodumène et pegmatites fortement albitisées à spodumène et à cassitérite de la région de Katumba (Ruanda). *Annales de la Société Géologique de Belgique*, 84: 257-278.

VARLAMOFF, N., 1963. Les phénomènes de greisenification, d'albitisation et de lépidolitisation et leurs relations spatiales avec les granites et les pegmatites granitiques d'Afrique. *Annales de la Société Géologique de Belgique*, 86: 285-322.

VARLAMOFF, N., 1969. Transitions entre les filons de quartz et les pegmatites stannifères de la région de Musha-Ntunga (Ruanda). *Annales de la Société Géologique de Belgique*, 92: 193-213.

VARLAMOFF, N., 1975. Classification des gisements d'étain. Académie Royale des sciences d'outre mer. *Classe des Sciences Naturelles et Médicales*, 19.

YURTSEVER, Y. & GAT, J.R., 1981. Atmospheric waters. *In* Gat, J.R. & Gonfiantini, R. (eds), *Stable Isotope Hydrology: Deuterium and Oxygen-18 in the Water Cycle*. International Atomic Energy Agency, Vienna, Technical Reports Series 210, 103–142.

WIJBRANS, J.R & MCDOUGALL, I., 1986., $^{40}Ar/^{39}Ar$ dating of white micas from an Alpine high pressure metamorphic belt on Naxos (Greece): the resetting of the argon isotopic system. *Contributions to Mineralogy and Petrology*, 93: 187–194.

WILKINSON, J.J., 1990. The role of metamorphic fluids in the development of the Cornubian orefield: fluid inclusion evidence from South Cornwall. *Mineralogical Magazine*, 54: 219-230.

WILKINSON, J.J., JENKIN, G.R.T., FALLICK, A.E. & FOSTER, R.P., 1995. Oxygen and hydrogen isotopic evolution of Varican crustal fluids, south Cornwall, UK. *Chemical Geology,* 123: 239-254.

WILLIS-RICHARDS, J.W. & JACKSON, N.J., 1989. Evolution of the Cornubian Ore field, Southwest England: Part I. Batholith modelling and ore distribution. *Economic Geology,* 84: 1078-1100.

ZHAO, Z.-F., ZHENG, Y.-F., WEI, C.-S., & GONG, B., 2004. Temporal relationship between granite cooling and hydrothermal uranium mineralization at Dalongshan in China: a combined radiometric and oxygen isotopic study. *Ore Geology Reviews*, 25: 221-236.

(manuscript received 25.10.2009, accepted in revised form 30.09.2009, available on line 15.10.2009)

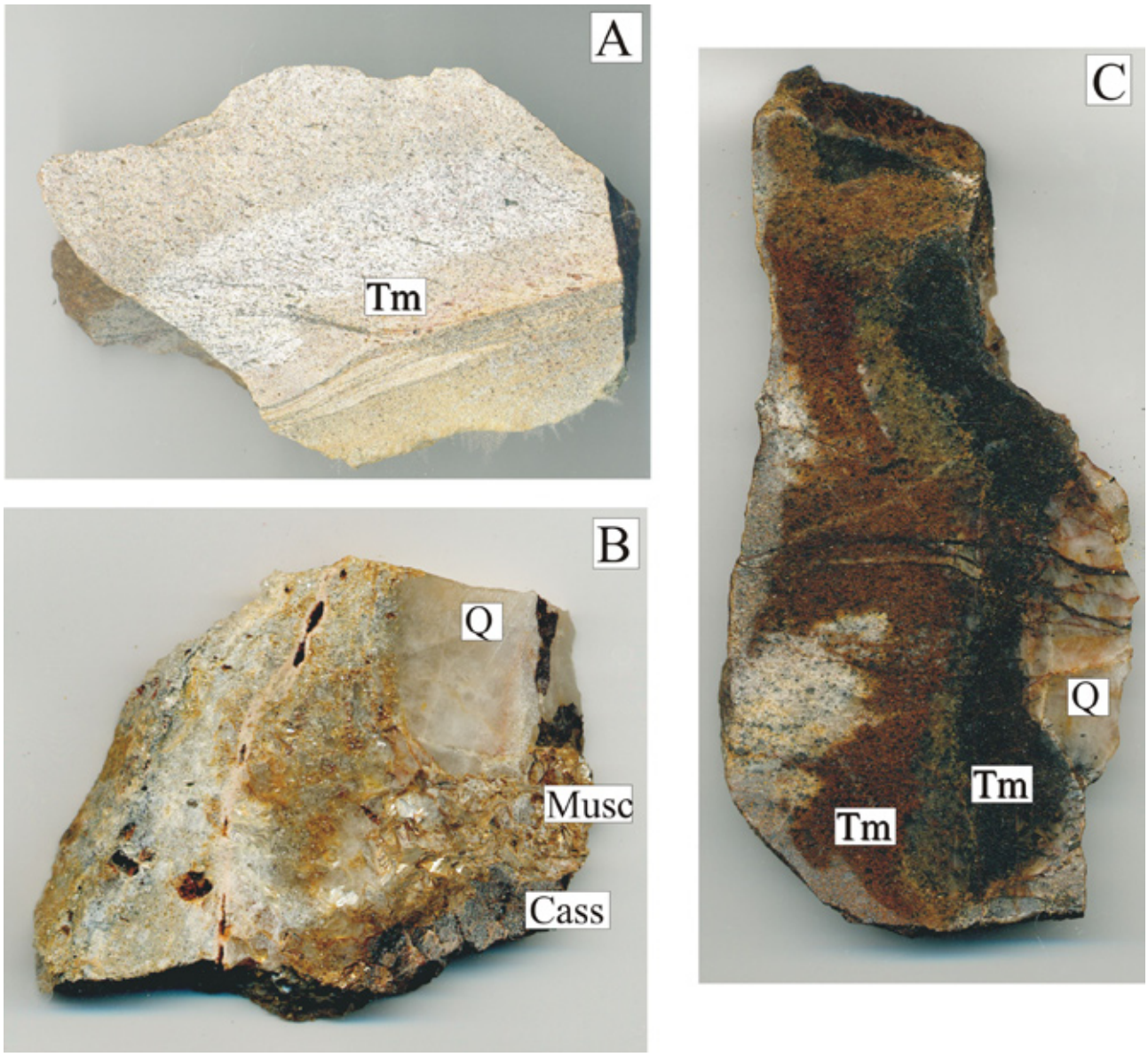

Plate 1.

A. Handpiece of Masoro (RG132997), showing the crystallisation of tourmaline crystals (TM) along cleavage planes. Sample width is ~10cm.
B. Mineralised quartz (Q) vein from Nyamiumba, with cassiterite (Cass) associated with muscovite (Musc). Sample width is ~15cm
C. Quartz vein with an alteration halo from Mahaza (RG 133021), showing a decrease in tourmaline (TM) away from the quartz vein (Q). Sample width is ~10cm.

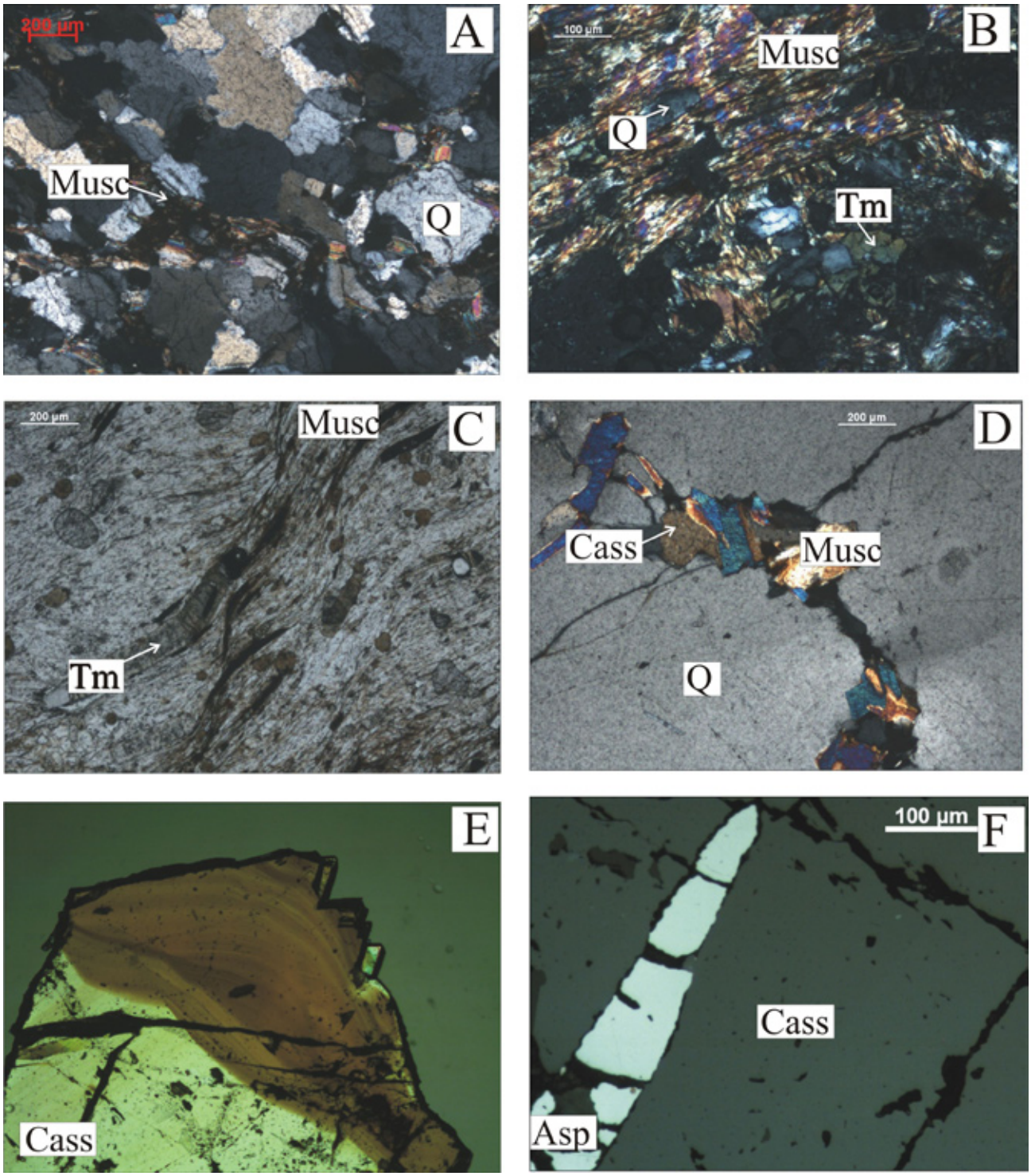

Plate 2.

A. Compacted quartzite forming the host-rock of Sn-mineralisation at Masoro, showing compacted and fractured quartz grains (Q), associated with muscovite (Musc). Sample: Masoro RG132964. Transmitted light.

B. Host-rock of Sn-mineralisation, showing muscovite (Musc), tourmaline (Tm) and quartz (Q). Sample: Mahaza RG133307. Transmitted light.

C. Host-rock of Sn-mineralisation showing growth of a tourmaline crystal (Tm), following a foliation plane consisting of muscovite (Musc). Sample: Masoro RG132990. Transmitted light.

D. Fracture in quartz vein, which is filled with cassiterite (Cass) and muscovite (Musc). Sample Masoro: RG132990. Transmitted light.

E. Wafer of a cassiterite crystal (~1cm wide) from Nyamiumba, showing nice colour zonation. Transmitted light.

F.. Microphotograph showing an arsenopyrite crystal (Asp) occurring in a fracture in a cassiterite crystal (Cass). Reflected light.